

Appendix S

Solutions

Chapter 1. Overture

Solution 1.1 - 3-disk symbolic dynamics. There are 2^k topologically different k -step trajectories starting from each disk, and the 3-disk pinball has $3 \cdot 2^{n-1}$ periodic points with length n itineraries composed of disk labels $\{1, 2, 3\}$.

As explained in sect. 1.4, each orbit segment can be characterized by either of the two symbols 0 and 1, differentiating topologically bouncing back or going onto the third disk.

Prime cycles in the 3-disk space (prime cycles in fundamental domain, respectively) are

- Of length 2: 12,13,32 (or 0).
- Of length 3: 123,321 (or 1).
- Of length 4: 1213,1232,1323 (or 01).
- Of length 5: 12123,12132,12313,12323,13132,13232 (or 00111).

Some of the cycles are listed in table 12.2 and drawn in figure ??.

(Y. Lan)

Solution 1.1 - 3-disk symbolic dynamics. Starting from a disk we cannot end up at the same disk in the next step, see figure S.1. We have 3 choices for the first disk and 2 choices for the next disk at each step, hence at most $3 \cdot 2^{n-1}$ itineraries of length n

Thus, it remains to show that any symbol sequence with the only constraint of no two identical consecutive symbols is realized. The most convenient way to do so is to work with the phase space representation of the pinball machine. Parametrize the state right after a reflection by the label of the disk, the arc length parameter corresponding to the point of reflection, and the $\sin \phi$ with ϕ being the angle of reflection relative to the normal vector, see figure S.1. Thus the Poincaré section consists of three cylinders, with the arc length parameter is cyclic on each disk, as shown in figure S.2.

Consider disk "1" as the starting point. Fixing the angle of reflection, by varying the position all the way around the disk we first escape, then hit disk "3", then

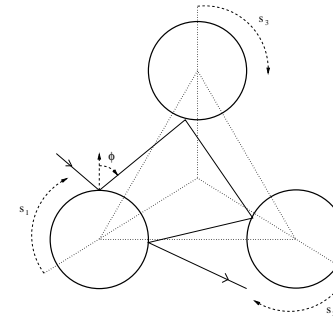


Figure S.1: Geometry of the 3-disk pinball.

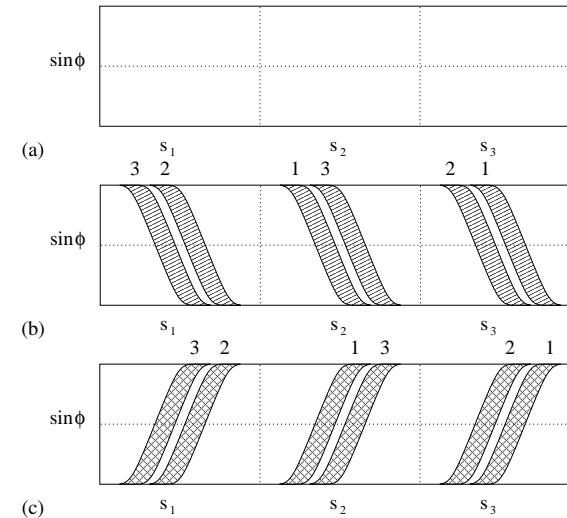


Figure S.2: (a) The phase space of the 3-disk pinball. (b) The part of phase space which remains on the table for one more iterate. (c) The images of the disks in one iteration.

escape, then hit disk "2", and then escape again, when increasing the arc length parameter in the manner indicated in figure S.1 (a). Thus—if the disks are sufficiently well separated—there are two strips of initial conditions which do not escape. By symmetry this yields figure S.1 (b) where the numbers indicate onto which disk these initial trajectories are going to end up on. By time reversal Figure S.1 (c) shows the strips labeled by disk where the pinball came from.

Combining figure S.1 (b) and (c) we obtain three sections, which are the same except for the labeling of the disks. One of such section is shown in figure S.3.

The billiard map enjoys a certain monotonicity, as depicted in figure S.4, which

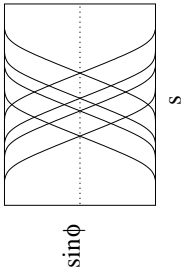


Figure S.3: The intersection of one iterate images and preimages.

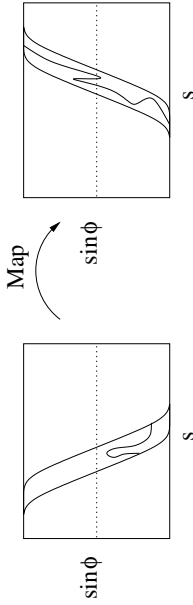


Figure S.4: Monotonicity of the billiard map.

easily verified by inspecting figure S.1. It says that any curve connecting the two boundaries of one of the strips gets mapped to a curve within the image of that strip running all the way across from top to bottom.

This, in particular, means that the intersections of the image of the previous disk and the initial conditions to land onto the next disk, see figure S.3, will map onto (thin) strips running across from top to bottom, as shown in figure S.5.

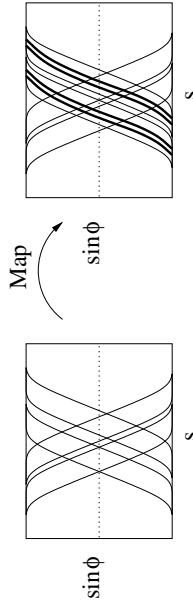


Figure S.5: Images in the second iterate. This is, of course, schematically, because we dropped the labels of the disks; in fact, the two intersection regions get mapped onto two different disks.

Finally, since the images of the intersection regions run all the way across in the vertical direction, we can iterate the argument. Every time the number of strips doubles, and we find regions of states which can go to either of the two neighboring disks at every step. Hence any symbol sequence with no repeat of consecutive symbols can be realized.

The itineraries of periodic points of period 2, 3, 4, 5 are

n	all periodic cycles
2	12 13 21 23 31 32
3	123 132 213 231 312 321
4	1212 1213 1232 1312 1313 1323 2121 2123 2131 2313 2321 2323 3121 3131 3132 3212 3231 3232
5	12123 12132 12312 12313 12323 13123 13132 13212 13213 13232 21213 21231 21313 21321 21323 23121 23123 23131 23213 23231 31212 31231 31232 31312 31321 32121 32131 32132 32312 32321

The prime cycles (lexically/lowest periodic point itinerary within a non-repeating cycle) are indicated in bold, and the ones given in the exercise are sketched in figure S.6.

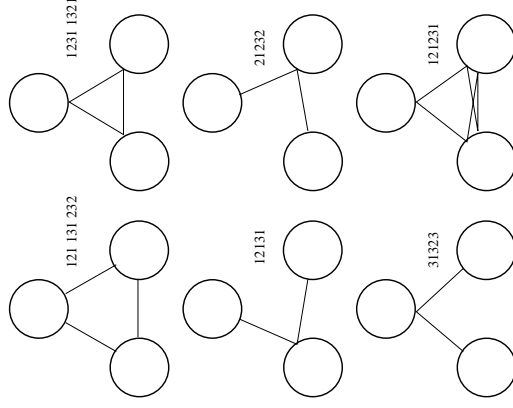


Figure S.6: Sketch of the indicated prime cycles.

(Alexander Grigo)

Solution 1.2 - Sensitivity to initial conditions. To estimate the pinball sensitivity we consider a narrow beam of point particles bouncing between two disks, figure S.7 (a). Or if you find this easier to visualize, think of a narrow ray of light. We assume that the ray of light is focused along the axis between the two points. This is where the least unstable periodic orbit lies, so its stability should give us an upper bound on the number of bounces we can expect to achieve. To estimate the stability we assume that the ray of light has a width $w(t)$ and a "dispersion angle" $\theta(t)$ (we assume both are small), figure S.7 (b). Between bounces the dispersion angle stays constant while the width increases as

$$w(t) \approx w(t') + (t - t')\theta$$

The outside edges of the ray of light will miss the disk when the width of the ray exceeds 2 cm; this occurs after 11 bounces.

(Adam Prügel-Bennett)

Solution 1.2 - Sensitivity to initial conditions, another try. Adam's estimate is not very good - do you have a better one? The first problem with it is that the instability is very underestimated. As we shall check in exercise 13.7, the exact formula for the 2-cycle stability is $\Lambda = R - 1 + R\sqrt{1 - 2/R}$. For $R = 6$, $a = 1$ this yields $w_n/w_0 \approx (5 + 2\sqrt{6})^n = 9.898979^n$, so if that were the whole story, the pinball would be not likely to make it much beyond 8 bounces.

The second problem is that local instability overestimates the escape rate from an enclosure; trajectories are reinjected by scatterers. In the 3-disk pinball the particle leaving a disk can be reinjected by hitting either of other 2 disks, hence $w_n/w_0 \approx (9.9/2)^n$. This interplay between local instability and global reinjection will be cast into the exact formula involving "Lyapunov exponent" and "Kolmogorov entropy". In order to relate this estimate to our best continuous time escape rate estimate $\gamma = 0.4103\dots$ (see table 20.2), we will have to also compute the mean free flight time (20.24). As a crude estimate, we take the shortest disk-to-disk distance, $\langle l \rangle = R - 2 = 4$. The continuous time escape rate result implies that $w_n/w_0 \approx e^{(\gamma - 2)nt} = (5.16)^n$, in the same ballpark as the above expansion-reinjection estimate. (P. Cvitanovic)

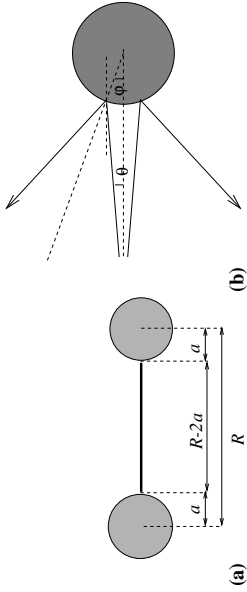


Figure 5.7: The 2-disk pinball (a) geometry, (b) defocusing of scattered rays.

At each bounce the width stays constant while the angle increases by

$$\theta_{n+1} = \theta_n + 2\phi \approx \theta_n + w(t)/a,$$

where θ_n denotes the angle after bounce n . Denoting the width of the ray at the n th bounce by w_n , then we obtain the pair of coupled equations

$$w_{n+1} = w_n + (R - 2a)\theta_n \tag{S.1}$$

$$\theta_n = \theta_{n-1} + \frac{w_n}{a} \tag{S.2}$$

where we ignore corrections of order w_n^2 and θ_n^2 . Solving for θ_n we find

$$\theta_n = \theta_0 + \frac{1}{a} \sum_{j=1}^n w_j.$$

Assuming $\theta_0 = 0$ then

$$w_{n+1} = w_n + \frac{R - 2a}{a} \sum_{j=1}^n w_j$$

Plugging in the values in the question we find the width at each bounce in Angstroms grows as 1, 5, 29, 169, 985, etc. To find the asymptotic behavior for a large number of bounces we try an solution of the form $w_n = a^n x^n$. Substituting this into the equation above and ignoring terms that do not grow exponentially we find solutions

$$w_n \approx a w_n^{asym} = a(3 \pm 2\sqrt{2})^n$$

The solution with the positive sign will clearly dominate. The constant a we cannot determine by this local analysis although it is clearly proportional to w_0 . However, the asymptotic solution is a good approximation even for quite a small number of bounces. To find an estimate of a we see that w_n/w_n^{asym} very rapidly converges to 0.146447, thus

$$w_n \approx 0.146447 w_0 (3 + 2\sqrt{2})^n \approx 0.1 \times w_0 \times 5.83^n$$

Chapter 2. Go with the flow

Solution 2.1 - Trajectories do not intersect. Suppose that two trajectories C_x and C_y intersect at some point z . We claim that any points \bar{x} on C_x is also a point on C_y and vice versa. We only need to prove the first part of the statement.

According to the definition of C_x , there exist $t_x, t_y, t_1 \in \mathbb{R}$ such that $f^{t_x}(x) = z, f^{t_y}(y) = z, f^{t_1}(x) = \bar{x}$. It is easy to check that $f^{t_x - t_1}(y) = \bar{x}$. So, $\bar{x} \in C_y$. Therefore, if two trajectories intersect, then they are the same trajectory. (Y. Lan)

Solution 2.2 - Evolution as a group. Let's check the basic defining properties of a group. The members of the set are $f^t, t \in \mathbb{R}$ and the "product law" is given by \circ :

- As $f^{t+s} = f^t \circ f^s$, the set is closed, i.e., the product of any two members generates another member of the set.
- It is associative, as $(f^t \circ f^s) \circ f^r = f^{t+s+r} = f^t \circ (f^s \circ f^r)$.
- $I = f^0$ is the identity, as $f^t \circ f^0 = f^t = f^0 \circ f^t$.
- f^{-t} is the inverse of f^t , as $f^{-t} \circ f^t = I$.

So, $\{f^t, t \in \mathbb{R}\}$ forms a group. As $f^t \circ f^s = f^{t+s} = f^s \circ f^t$, it is a commutative (Abelian) group.

Any Abelian group can replace the continuous time. For example, \mathbb{R} can be replaced by \mathbb{Z}_6 . To mess things up try a non-commutative group. (Y. Lan)

Solution 2.3 - Almost ODE's. What is an ODE on \mathbb{R} ? An ODE is an equality which reveals explicitly the relation between function $x(t)$ and its time derivatives \dot{x}, \ddot{x}, \dots , i.e., $F(t, x, \dot{x}, \ddot{x}, \dots) = 0$ for some given function F . Let's check the equations given in the exercise.

- (a) $\dot{x} = \exp(\dot{x})$ is an ODE.
- (b) $\dot{x} = x(x(t))$ is not an ODE, as $x(t(t))$ is not a known function acting on $x(t)$.
- (c) $\dot{x} = x(t+1)$ is not an ODE, as $x(t+1)$ is not a value at current time. Actually, it is a difference-differential equation. (Y. Lan)

Solution 2.4 - All equilibrium points are fixed points. Given a vector field $v(x)$, the state space dynamics is defined by

$$\frac{d}{dt}x(t) = v(x(t)). \quad (\text{S.3})$$

An equilibrium point a of v is defined by $v(a) = 0$, so $x(t) = a$ is a constant solution of (S.3). For the flow f^t defined by (S.3), this solution satisfies $f^t(a) = a, t \in \mathbb{R}$. So, it is a fixed point of the dynamics f^t . (Y. Lan)

Solution 2.5 - Gradient systems.

1. The directional derivative

$$\frac{d}{dt}\phi = n \cdot \nabla\phi$$

produces the increasing rate along the unit vector n . So, along the gradient direction $\nabla\phi/|\nabla\phi|$, ϕ has the largest increasing rate. The velocity of the particle has the opposite direction to the gradient, so ϕ decreases most rapidly in the velocity direction.

2. An extremum a of ϕ satisfies $\nabla\phi(a) = 0$. According to exercise 2.4, a is a fixed point of the flow.

3. Two arguments lead to the same conclusion here.

First, near an equilibrium point, the equation is always linearizable. For gradient system, after orthogonal transformation it is even possible to write the linearized equation in diagonal form so that we need only to consider one eigen-direction. The corresponding scalar equation is $\dot{x} = \lambda x$. Note that we moved the origin to the equilibrium point. The solution of this equation is $x(t) = x(0)\exp(\lambda t)$, for $\lambda \neq 0$. If $x(0) \neq 0$, it will take infinite amount of time (positive or negative) for $x(t) \rightarrow 0$. For $\lambda = 0$, the approach to zero is even slower as then only higher orders of x take effect.

The second argument seems easier. We know that the solution curve through an equilibrium point is the point itself. According to exercise 2.1, no other solution curve will intersect it, which means that if not starting from the equilibrium point itself, other point can never reach it.

4. On a periodic orbit, the velocity is bounded away from zero. So ϕ is always decreasing on a periodic orbit, but in view of the periodicity, we know that this can not happen (at each point, there is only one value of ϕ). So, there is no periodic orbit in a gradient system.

(Y. Lan)

Solution 2.7 - Rössler system. You will probably want the matlab function `ode45` to do this. There are several others which perform better in different situations (for example `ode23` for stiff ODEs), but `ode45` seems to be the best for general use.

To use `ode45` you must create a function, say `rossler`, which will take in a time and a vector of $[x, y, z]$ and return $[xdot, ydot, zdot]$. Then the command would be something like

```
ode45(@rossler, [tmin, tmax], [x0 y0 z0], @rossler)
```

(Jonathan Halcrow)

Solution 2.8 - Equilibria of the Rössler system.

1. Solve $\dot{x} = \dot{y} = \dot{z} = 0$, to get $x = az, y = -z$ and $x^2 - cx + ab = 0$. There are two solutions of a quadratic equation, hence there are two equilibrium points:

$$x^\pm = az^\pm = -ay^\pm = (c \pm \sqrt{c^2 - 4ab})/2.$$

2. The above expressions are exact. However, it pays to think of $\epsilon = a/c$ as a small parameter in the problem. By substitution from exercise 2.8,

$$x^\pm = cp^\pm, y^\pm = -p^\pm/\epsilon, z^\pm = p^\pm/\epsilon. \quad (\text{S.4})$$

Expanding \sqrt{D} in ϵ yields $p^- = \epsilon^2 + a(\epsilon^3)$, and $p^+ = 1 - \epsilon^2 + o(\epsilon^3)$. Hence

$$\begin{aligned} x^- &= a^2/c + o(\epsilon^3), & x^+ &= c - a^2/c + o(\epsilon^3), \\ y^- &= -a/c + o(\epsilon^2), & y^+ &= c/a + a/c + o(\epsilon^2), \\ z^- &= a/c + o(\epsilon^2), & z^+ &= c/a - a/c + o(\epsilon^2). \end{aligned} \quad (\text{S.5})$$

For $a = b = 0.2$, $c = 5.7$ in (2.17), $\epsilon \approx 0.035$, so

$$\begin{aligned}(x^-, y^-, z^-) &= (0.0070, -0.0351, 0.0351), \\ (x^+, y^+, z^+) &= (5.6929, -28.464, 28.464).\end{aligned}\tag{S.6}$$

(R. Paškauskas)

Solution 2.10 - Classical collinear helium dynamics. An example of a solution are A. Prügel-Bennett's programs, available at ChaosBook.org/extras.

Chapter 3. Discrete time dynamics

(No solutions available.)

Chapter 4. Local stability

Solution 4.1 - Trace-log of a matrix. 1) Consider $M = \exp A$.

$$\det M = \det \lim_{n \rightarrow \infty} \left(\mathbf{1} + \frac{1}{n} A \right)^n = \lim_{n \rightarrow \infty} \left(\mathbf{1} + \frac{1}{n} \operatorname{tr} A + \dots \right)^n = \exp(\operatorname{tr}(\ln M))$$

2) A rephrasing of the solution 1): evaluate $\frac{d}{dt} \det(e^{t \ln M})$ by definition of derivative in terms of infinitesimals. (Kasper Juel Eriksen)

3) Here is an example of wrong/incomplete answer, hiding behind fancier notation: This identity makes sense for a matrix $M \in \mathbb{C}^{n \times n}$, if $\prod_{i=1}^n |\lambda_i| < \infty$ and $\prod_{i=1}^n |\lambda_i| > 0$, $\forall i$, where $\{\lambda_i\}$ is a set of eigenvalues of M . Under these conditions there exist a nonsingular $O: M = O D O^{-1}$, $D = \operatorname{diag}\{\lambda_i, i = 1, \dots, n\}$. If $f(M)$ is a matrix valued function defined in terms of power series then $f(M) = O f(D) O^{-1}$, and $f(D) = \operatorname{diag}\{f(\lambda_i)\}$. Using these properties and cyclic property of the trace we obtain

$$\exp(\operatorname{tr}(\ln M)) = \exp \left(\sum_i \ln \lambda_i \right) = \prod_i \lambda_i = \det(M)$$

What's wrong about it? If a matrix with degenerate eigenvalues, $\lambda_i = \lambda_j$ is of Jordan type, it cannot be diagonalized, so a bit more of discussion is needed to show that the identity is satisfied by upper-triangular matrices.

4) First check that this is true for any Hermitian matrix M . Then write an arbitrary complex matrix as sum $M = A + iB$, A, B Hermitian. Taylor expand in z and prove by analytic continuation that the identity applies to arbitrary M . (David Mermin)

5) check appendix J.1

Solution 4.2 - Stability, diagonal case. The relation (4.17) can be verified by noting that the defining product (4.13) can be rewritten as

$$\begin{aligned} e^{tA} &= \left(\mathbf{U} \mathbf{U}^{-1} + \frac{t \mathbf{U} \mathbf{A}_D \mathbf{U}^{-1}}{m} \right) \left(\mathbf{U} \mathbf{U}^{-1} + \frac{t \mathbf{U} \mathbf{A}_D \mathbf{U}^{-1}}{m} \right) \dots \\ &= \mathbf{U} \left(\mathbf{I} + \frac{t \mathbf{A}_D}{m} \right) \mathbf{U}^{-1} \mathbf{U} \left(\mathbf{I} + \frac{t \mathbf{A}_D}{m} \right) \mathbf{U}^{-1} \dots = \mathbf{U} e^{t \mathbf{A}_D} \mathbf{U}^{-1}. \end{aligned} \quad (\text{S.7})$$

Solution 4.3 - State space volume contraction.

(a) The Rössler flow volume contraction rate at the equilibria follows from $\partial_t \nu = x + a - c = x - 5.5$; $\partial_t \nu_- = -5.493$, $\partial_t \nu_+ = +0.1929$.

(b,c) The result is obvious and uninteresting. The point of the exercise is that the instantaneous velocity gradients matrix velocity gradients matrix gives no information about recurrent dynamics, what you want to color code are the eigenvalues of the finite time J^{at} Poincaré section returns.

(d) The average contraction rate (4.47) along a typical trajectory on the Rössler attractor is something like $\langle \partial_t \nu \rangle = -5.3$ (Li, after 10^5 iterations); -5.319 (Ding, after ? iterations); -5.3302 (Daniel, after 10^5 iterations); -5.36545648709 (Nah, unexplained procedure). Its plot as a function of time illustrates one problem of time-averaging in chaotic flows - it varies widely across each recurrence to a given Poincaré section. Even if it were worth your while to know its numerical value, the contraction rate cannot be linked to a computable fractal dimension. The relation goes through expanding eigenvalues, sect. 5.4. As the contraction is of order of 10^{-15} , there is no numerical algorithm that would give you any fractal dimension other than $D_H = 1$ for this attractor.

(e) (any argument tends to be good enough).

(f) The average contraction on the escape side of the outer equilibrium: not available.

Solution 4.4 - Topology of the Rössler flow.

1. The characteristic determinant of the stability matrix that yields the equilibrium point stability (4.31) yields

$$\begin{vmatrix} -\lambda & -1 & -1 \\ 1 & a - \lambda & 0 \\ z^2 & 0 & x^2 - c - \lambda \end{vmatrix} = 0$$

$$\lambda^3 + \lambda^2(-a - x^2 + c) + \lambda(a(x^2 - c) + 1 + x^2/a) + c - 2x^2 = 0.$$

Equation (4.59) follows after noting that $x^2 - c = c(p^2 - 1) = -c p^2$ and $2x^2 - c = c(2p^2 - 1) = \pm c \sqrt{D}$, see (2.8).

2. Approximate solutions of (4.59) are obtained by expanding p^2 and \sqrt{D} and substituting into this equation. Namely,

$$\begin{aligned} \sqrt{D} &= 1 - 2\epsilon^2 - 2\epsilon^4 - 4\epsilon^6 - \dots \\ p^+ &= \epsilon^2 + \epsilon^4 + 2\epsilon^6 + \dots \\ p^- &= 1 - \epsilon^2 - \epsilon^4 - 2\epsilon^6 + \dots \end{aligned}$$

In case of the equilibrium " u_- ", close to the origin expansion of (4.59) results in

$$(x^2 + 1)(\lambda + c) = -\epsilon \lambda (1 - \epsilon^2 - c\lambda) + \epsilon^2 c(\lambda^2 + 2) + o(\epsilon^2)$$

The term on the left-hand side suggests the expansion for eigenvalues as

$$\lambda_i = -c + \epsilon a_i + \dots, \quad \lambda_2 + i\theta_2 = \epsilon b_1 + i + \dots$$

after some algebra one finds the first order correction coefficients $a_1 = c/(c^2 + 1)$ and $b_1 = (c^3 + i)/(2(c^2 + 1))$. Numerical values are $\lambda_1 \approx -5.694$, $\lambda_2 + i\theta_2 \approx 0.0970 + i1.0005$.

In case of p^+ , the leading order term in (4.59) is $1/\epsilon$. Set $x = \lambda/\epsilon$, then expansion of (4.59) results in

$$x = c - \epsilon x - \epsilon^2(2c - x) - \epsilon^3(x^3 - c x^2) - \epsilon^4(2c - x)(1 + c^2) + c x^2 + o(\epsilon^4)$$

Solve for real eigenvalue first. Set $x = c + \epsilon a_1 + \epsilon^2 a_2 + \epsilon^3 a_3 + \epsilon^4 a_4 + \dots$. The subtle point here is that leading order correction term of the real eigenvalue is ϵa_1 , but to determine leading order of the real part of complex eigenvalue, one needs all terms a_i through a_4 .

$$\begin{aligned} \epsilon^0: & a_1 + c = 0 & a_1 &= -c \\ \epsilon^1: & c + a_1 + a_2 = 0 & a_2 &= 0 \\ \epsilon^2: & a_1 - a_2 - a_3 = 0 & a_3 &= -c \\ \epsilon^4: & c + c^2 a_1 - a_2 + a_3 + a_4 = 0 & a_4 &= c^3. \end{aligned}$$

hence

$$\mu^{(1)} = \epsilon x = a - a^2/c + o(\epsilon^3) \approx 0.192982.$$

To calculate the complex eigenvalue, one can make use of identities $\det A = \prod \lambda = 2x^3 - c$, and $\text{tr} A = \sum \lambda = a + x^3 - c$. Namely,

$$\begin{aligned} \lambda_2 &= \frac{1}{2}(a - c)^{-} - \lambda_1) = -\frac{a^2}{2c} + o(\epsilon^5) \approx -0.49 \times 10^{-6}, \\ \theta_2 &= \sqrt{\frac{2c^2 - 3}{4c} - \lambda_2^2} = \sqrt{\frac{4ac}{4c}} (1 + o(\epsilon)) \approx 5.431. \end{aligned}$$

(R. Paškauskas)

Chapter 5. Cycle stability

Solution 5.1 - A limit cycle with analytic Floquet exponent. The 2 - dimensional flow is cooked up so that $x(t) = (q(t), p(t))$ is separable (check!) in polar coordinates $q = r \cos \phi$, $p = r \sin \phi$:

$$\dot{r} = r(1 - r^2), \quad \dot{\phi} = 1. \tag{S.8}$$

In the (r, ϕ) coordinates the flow starting at any $r > 0$ is attracted to the $r = 1$ limit cycle, with the angular coordinate ϕ wrapping around with a constant angular velocity $\omega = 1$. The non-wandering set of this flow consists of the $r = 0$ equilibrium and the $r = 1$ limit cycle.

Equilibrium stability: As the change of coordinates is defined everywhere except at the equilibrium point ($r = 0$, any ϕ), the equilibrium stability matrix (4.31) has to be computed in the original (q, p) coordinates,

$$A = \begin{bmatrix} 1 & 1 \\ -1 & 1 \end{bmatrix}. \tag{S.9}$$

The eigenvalues are $\lambda = \mu \pm i \omega = 1 \pm i$, indicating that the origin is linearly unstable, with nearby trajectories spiralling out with the constant angular velocity $\omega = 1$. The Poincaré section ($p = 0$, for example) return map is in this case also a stroboscopic map, strobed at the period (Poincaré section return time) $T = 2\pi/\omega = 2\pi$. The radial Floquet multiplier per one Poincaré return is $|\lambda| = e^{\mu T} = e^{2\pi}$.

Limit cycle stability: From (S.8) the stability matrix is diagonal in the (r, ϕ) coordinates,

$$A = \begin{bmatrix} 1 - 3r^2 & 0 \\ 0 & 0 \end{bmatrix}. \tag{S.10}$$

The vanishing of the angular $\lambda^{(0)} = 0$ eigenvalue is due to the rotational invariance of the equations of motion along ϕ direction. The expanding $\lambda^{(1)} = 1$ radial eigenvalue of the equilibrium $r = 0$ confirms the above equilibrium stability calculation. The contracting $\lambda^{(1)} = -2$ eigenvalue at $r = 1$ decreases the radial deviations from $r = 1$ with the radial Floquet multiplier $\Lambda_r = e^{\mu T} = e^{-4\pi}$ per one Poincaré return. This limit cycle is very attracting.

Stability of a trajectory segment: Multiply (S.8) by r to obtain $\frac{1}{2}\dot{r}^2 = r^2 - r^4$, set $r^2 = 1/u$, separate variables $du/(1-u) = 2 dt$, and integrate: $\ln(1-u) - \ln(1-u_0) = -2t$. Hence the $r(t_0, t)$ trajectory is

$$r(t)^2 = 1 + (r_0^2 - 1)e^{-2t}. \tag{S.11}$$

The $[1 \times 1]$ Jacobian matrix

$$J(r_0, t) = \left. \frac{\partial r(t)}{\partial r_0} \right|_{t_0=r_0}. \tag{S.12}$$

Chapter 6. Get straight

Solution 6.1 - Harmonic oscillator in polar coordinates. Harmonic oscillator equations in Cartesian coordinates are

$$\dot{p} = -q, \quad \dot{q} = p. \quad (\text{S.14})$$

In polar form, we write

$$q = r \cos \theta, \quad p = r \sin \theta. \quad (\text{S.15})$$

The inverse of the Jacobian $\frac{\partial(q,p)}{\partial(r,\theta)}$ of this transformation is

$$\frac{\partial(r,\theta)}{\partial(q,p)} = \begin{pmatrix} \cos \theta & \sin \theta \\ -\frac{1}{r} \sin \theta & \frac{1}{r} \cos \theta \end{pmatrix}, \quad (\text{S.16})$$

leading to

$$\begin{pmatrix} \dot{r} \\ \dot{\theta} \end{pmatrix} = \begin{pmatrix} \cos \theta & \sin \theta \\ -\frac{1}{r} \sin \theta & \frac{1}{r} \cos \theta \end{pmatrix} \cdot \begin{pmatrix} \dot{q} \\ \dot{p} \end{pmatrix} = \begin{pmatrix} 0 \\ -1 \end{pmatrix} \quad (\text{S.17})$$

(R. Witczak)

Solution 6.2 - Coordinate transformations. (No solution available.)

Solution 6.3 - Linearization for maps. (difficulty: medium) The first few terms of the map h that conjugates f to αz

$$f(z) = h^{-1}(\alpha h(z)).$$

are determined many places, for example in ref. [16.9].

There are conditions on the derivative of f at the origin to assure that the conjugation is always possible. These conditions are formulated in ref. [1.26], among others.

Solution 6.4 - Ulam and tent maps. This conjugacy is derived in many introductory chaos textbooks: see, for example, ref. [6.11] for a detailed discussion.

satisfies (4.9)

$$\frac{d}{dt} J(r,t) = A(r)J(r,t) = (1 - 3r(t)^2)J(r,t), \quad J(r_0,0) = 1.$$

This too can be solved by separating variables $d(\ln J(r,t)) = dt - 3r(t)^2 dt$, substituting (S.11) and integrating. The stability of any finite trajectory segment is:

$$J(r_0,t) = (r_0^2 + (1 - r_0^2)e^{-2t})^{-3/2} e^{-2t}. \quad (\text{S.13})$$

On the $r = 1$ limit cycle this agrees with the limit cycle multiplier $\Lambda_r(1,t) = e^{-2t}$, and with the radial part of the equilibrium instability $\Lambda_r(r_0,t) = e^t$ for $r_0 \ll 1$. (P. Cvitanović)

Solution 5.2 - The other example of a limit cycle with analytic Floquet exponent. Email your solution to ChaosBook.org and G.B. Ermentrout.

Solution 5.3 - Yet another example of a limit cycle with analytic Floquet exponent. Email your solution to ChaosBook.org and G.B. Ermentrout.

Chapter 7. Newtonian dynamics

(No solutions available.)

Chapter 8. Billiards

Solution 8.1 - A pinball simulator. *Examples of pretty pinballs are A. Prügel-Bennett's `xpinball.c` and W. Benfold's java programs, available at ChaosBook.org/extras*

Solution 8.4 - Billiard exercises. *Korsch and Jodl [1.16] have a whole book of numerical exercises with billiards, including 3-disks.*

Solution 8.6 - Birkhoff coordinates. *Hint: compute the determinant of (8.11).*

Chapter 9. World in a mirror

Solution 9.1 - Polynomials invariant under discrete operations on \mathbb{R}^3 . See Gilmore and Letellier [9.14], Sect. 2.1.

Solution 9.2 - $G_x \subset G$. Keep in mind that the representation of $g_j \circ g_i$ is $g_j g_i$.

1. Closure: If $g_i, g_j \in G_x$, then $(g_j g_i)x = g_j(g_i x) = g_j x = x$ and thus $g_j \circ g_i \in G_x$.
2. Associativity: Trivial.
3. Identity e : $e x = x$ for any x and thus $e \in G_x$.
4. Inverse g_i^{-1} : For every $g \in G_x$, there exists a unique element $h = g^{-1} \in G$ such that $h \circ g = g \circ h = e$. We need to show $g^{-1} \in G_x$. Multiply $g x = x$ from the left with g^{-1} to get $g^{-1} g x = g^{-1} x$ or $g^{-1} x = x$ and thus $g^{-1} \in G_x$.

(Evangelos Siminos)

Solution 9.4 - Isotropy subgroup of g_x . For every $h \in G_{g_x}$, we have

$$h(g \cdot x) = g \cdot x$$

Multiplying from the left with g^{-1} and using associativity we get $(g^{-1} h g)x = x$ and thus $g^{-1} \circ h \circ g \in G_x$. Therefore x and $g x$ have conjugate isotropy subgroups.

Solution 9.6 - Reduction of 3-disk symbolic dynamics. The answer is given in sect. 21.6, see figure 9.6, figure 9.9, figure 12.12. Some remarks concerning part (c):

If an orbit does not have any spatial symmetry, its length in the fundamental domain is equal to that in the full space. One fundamental domain orbit corresponds to six copies of the orbit in the full space related to each other by symmetries. If a periodic orbit does have a spatial symmetry, then its fundamental domain image is a fraction of that in the whole space, and the orbit (and its symmetry partners) in the full space is tiled by copies of the relative periodic orbit, corresponding to an orbit in the fundamental domain. The higher symmetry an orbit has, the shorter the relative periodic orbit.

Another way to visualize a fundamental domain orbit: put a periodic orbit and all its spatial symmetry relatives simultaneously in the full space. The segments that fall into a fundamental domain constitute the orbit in the fundamental domain. (Y. Lan)

Solution 12.6 - 3-disk fundamental domain symbolic dynamics. Read sect. 1.4.

Solution 9.8 - Lorenz system in polar coordinates: group theory. No solution available.

Solution 9.9 - Proto-Lorenz system. This exercise is based on Miranda and Stone [9.12]; their paper gives a detailed discussion.

1. The proto-Lorenz equation, (2.12), in terms of variables $(u, v, z) = (x^2 - y^2, 2xy, z)$:

$$\begin{bmatrix} \dot{u} \\ \dot{v} \\ \dot{z} \end{bmatrix} = \begin{bmatrix} -(\sigma + 1)u + (\sigma - r)v + (1 - \sigma)N + v z \\ (r - \sigma)u - (\sigma + 1)v + (r + \sigma)N - uz - uN \\ v/2 - bz \end{bmatrix} \quad N = \sqrt{u^2 + v^2}. \quad (\text{S.18})$$

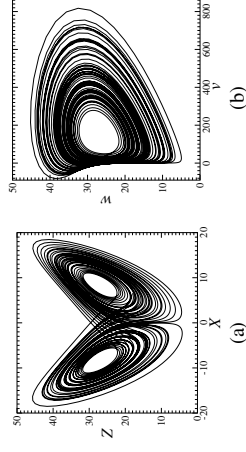


Figure S.8: (a) The Lorenz attractor. (b) The Rössler-like proto-Lorenz attractor, with points related by rotation symmetry about the z -axis identified. (From ref. [H.8].)

4. The equilibria of proto-Lorenz: origin the same, $(u, v, z) = (0, 0, 0)$. The R -symmetric pair (2.13) is now a single equilibrium at

$$hE_0 = (0, 2b(r-1), r-1). \quad (\text{S.19})$$

Chapter 10. Continuous symmetries

Solution 10.1 - Visualizations of the 5-dimensional complex Lorenz flow. A numerical solution of the set of ODEs (10.2) is obtained by using the `Mathematica` `NDSolve` function, for t from 0 to 100 and setting the initial (x_1, x_2, y_1, y_2, z) to some arbitrary value. We set `MaxSteps` \rightarrow `Infinity` in order to resolve the fine structure of the flow. The solution is then plotted by means of `ParametricPlot3D`, in any three of the five $\{x_1, x_2, y_1, y_2, z\}$ axes. Figure 10.1 illustrates the shape of the attractor projected onto the $\{x_1, x_2, z\}$ subspace, with (10.2) parameter values. Projections onto $\{y_1, y_2, z\}$ and other subspaces are visually similar, and seem not to offer additional insights into dynamics of this system.

Here is a `Mathematica` program that generates a long-time plot of complex Lorenz equations, such as figure 10.1, initiated from a point on the attractor (after this integration, the initial condition ic is the final point of the preceding integration):

```
v[t_]={-σ x1[t] + σ y1[t], -σ x2[t] + σ y2[t],
  (r1 - z[t])x1[t] - r2x2[t] - y1[t] - ey2[t],
  r2x1[t] + (r1 - z[t])x2[t] + ey1[t] - y2[t],
  -b z[t] + x1[t]y1[t] + x2[t]y2[t];
x[t_]= {x1[t], x2[t], y1[t], y2[t], z[t];
d=length[x[t]];
eqns=Table[D[x[t][[i]], t]==v[t][[i]], {i, 1, d}];
xde={x1, x2, y1, y2, z};
r1= 28; r2=0; b=8/3; e=1/10; σ=10;
tf= 80;
ic={x1[0]==0.867, x2[0]==-0.455, y1[0]==-0.552, y2[0]==0.453,
  z[0]==-22.4};
```

```
sol=NDSolve[eqns, ic], xde, {t, 0, tf}, MaxSteps  $\rightarrow$   $\infty$ ]/Flatten;
traj[t_]=x[t]/.sol;
pl=ParametricPlot3D[traj[t][[1]], traj[t][[2]], traj[t][[5]],
  {t, 0, tf}, PlotPoints  $\rightarrow$  400, PlotRange  $\rightarrow$  All]
ic=Table[x[0][[i]]==traj[tF][[i]], {i, 1, d}];
(R. Wilczak)
```

Solution 10.2 - A flow with two Fourier modes. (Solution not available.)

Solution 10.3 - SO(2) rotations in a plane. Expand $\exp(\theta \mathbf{T})$ as a power series, noting that

$$\mathbf{T}^2 = \begin{pmatrix} 0 & 1 \\ -1 & 0 \end{pmatrix} = -1.$$

See also example 4.5. (P. Cvitanović)

Solution 10.5 - U(1) equivariance of complex Lorenz equations for finite angles. Multiply the coordinates by a complex phase: $x \rightarrow e^{i\phi} x$, $y \rightarrow e^{i\phi} y$. Equivariance of (10.1) follows by inspection. If all coefficients are real, there is also a discrete C_2 symmetry under complex conjugation of the three equations. However, we consider here the cases where one or both of the parameters r and a are complex, breaking this discrete symmetry. (P. Cvitanović)

Solution 10.6 - SO(2) equivariance of complex Lorenz equations for finite angles. For this problem, the operation is rotation and $v(x)$ is given by (10.2). Rotation can be defined using the matrix $g(\theta)$ defined in (10.18), where θ is the angle of rotation. We need to verify that

$$v(x) = g^{-1} v(gx). \quad (\text{S.20})$$

First, the system is rotated as

$$\begin{pmatrix} \cos(\theta) & \sin(\theta) & 0 & 0 & 0 \\ -\sin(\theta) & \cos(\theta) & 0 & 0 & 0 \\ 0 & 0 & \cos(\theta) & \sin(\theta) & 0 \\ 0 & 0 & -\sin(\theta) & \cos(\theta) & 0 \\ 0 & 0 & 0 & 0 & 1 \end{pmatrix} \begin{pmatrix} x_1(t) \\ x_2(t) \\ y_1(t) \\ y_2(t) \\ z(t) \end{pmatrix}. \quad (\text{S.21})$$

The time derivative of the resulting matrix is taken, and then it is multiplied on the left by the inverse of the rotation matrix, giving

$$g^{-1} v(gx) = \begin{pmatrix} \sigma y_1(t) - \sigma x_1(t) \\ \sigma y_2(t) - \sigma x_2(t) \\ -r_2 x_2(t) - y_1(t) - e y_2(t) + x_1(0)(r_1 - z(t)) \\ r_2 x_1(t) + e y_1(t) - y_2(t) + x_2(0)(r_1 - z(t)) \\ x_1(t)y_1(t) + x_2(t)y_2(t) - b z(t) \end{pmatrix}, \quad (\text{S.22})$$

which is the same as the original system of ODEs, so that the system is rotationally equivariant for all finite angle rotations. (R. Wilczak)

Solution 10.7 - Stability matrix of complex Lorenz flow. The stability matrix (10.26), defined in (4.3), for complex Lorenz flow (10.2) can be computed by `Mathematica` program

```
v[t]= {x1'[t], x2'[t], y1'[t], y2'[t], z'[t]};
x[t]= {x1[t], x2[t], y1[t], y2[t], z[t]};
A = D[v[t], x[t], 1]
```

(R. Wilczak and P. Cvitanović)

Solution 10.8 - Rotational equivariance of complex Lorenz equations for infinitesimal angles. Now that we have the stability matrix (10.26), we can check the equivariance condition (10.24), $0 = -\mathbf{T} v(x) + A \mathbf{T} x$, where A is the stability matrix (4.3), by explicit substitution. The matrix \mathbf{T} is (10.17). Plugging these into (10.24), as well as using (10.2) for $v(x)$, the result is indeed 0, as expected. Then the system is rotationally equivariant for infinitesimal angles. (R. Wilczak)

Solution 10.9 - Discover the equivariance of a given flow? If M is in the Lie algebra, by the equivariance condition (10.24) the Lie derivative $M v(x) - A M x$ vanishes. You have $v(x)$ and the stability matrix A , hence try finding whether a M can be found such that the Lie derivative vanishes. You know that if the symmetry group is a subgroup of $SO(d)$, the Lie algebra elements M can be taken antisymmetric. (Have not tried to solve this problem, so let us know if you succeed) (P. Cvitanović)

Solution 10.10 - Equilibria of complex Lorenz equations. To find these points for complex Lorenz equations, I used the Solve function in Mathematica, with

$$\begin{pmatrix} \dot{x}_1(t) \\ \dot{x}_2(t) \\ \dot{y}_1(t) \\ \dot{y}_2(t) \\ \dot{z}(t) \end{pmatrix} = \begin{pmatrix} \sigma Y_1(t) - \sigma X_1(t) \\ \sigma Y_2(t) - \sigma X_2(t) \\ -r_2 X_2(t) - y_1(t) - e Y_2(t) + x_1(t)(r_1 - z(t)) \\ r_2 X_1(t) + e Y_1(t) - Y_2(t) + X_2(t)(r_1 - z(t)) \\ x_1(t)Y_1(t) + X_2(t)Y_2(t) - bZ(t) \end{pmatrix} = \begin{pmatrix} 0 \\ 0 \\ 0 \\ 0 \\ 0 \end{pmatrix}$$

as the equations defining the system, and then solved for $(x_1(t), x_2(t), y_1(t), y_2(t), z(t))$. Mathematica returns the point $(0, 0, 0, 0, 0)$ as the only solution, and thus (I hope, have no proof) the only equilibrium point. (R. Wilczak)

Solution 10.11 - Equilibria of complex Lorenz equations. See Siminos thesis [10.5].

Solution 10.12 - Complex Lorenz equations in polar coordinates. We use the same method here as in exercise 6.1. The Jacobian of this transformation can be written as

$$\frac{\partial(r_1, \theta_1, r_2, \theta_2, z)}{\partial(x_1, x_2, y_1, y_2, z)} = \begin{pmatrix} \cos(\theta_1) & \sin(\theta_1) & 0 & 0 & 0 \\ -\frac{\sin(\theta_1)}{r_1} & \frac{\cos(\theta_1)}{r_1} & 0 & 0 & 0 \\ 1 & 0 & 0 & 0 & 0 \\ 0 & 0 & \cos(\theta_2) & \sin(\theta_2) & 0 \\ 0 & 0 & -\frac{\sin(\theta_2)}{r_2} & \frac{\cos(\theta_2)}{r_2} & 0 \\ 0 & 0 & 0 & 0 & 1 \end{pmatrix}. \quad (\text{S.23})$$

Multiplying the velocity matrix on the left by the Jacobian (S.23), we get

$$\begin{pmatrix} \dot{r}_1 \\ \dot{\theta}_1 \\ \dot{r}_2 \\ \dot{\theta}_2 \\ \dot{z} \end{pmatrix} = \begin{pmatrix} -\sigma(r_1 - r_2 \cos \theta) \\ -\sigma \frac{r_1}{r_1} \sin \theta \\ -r_2 + r_1((\rho_1 - z) \cos \theta - \rho_2 \sin \theta) \\ e + \frac{r_1}{r_2}((\rho_1 - z) \sin \theta + \rho_2 \cos \theta) \\ -bz + r_1 r_2 \cos \theta \end{pmatrix},$$

where $\theta = \theta_1 - \theta_2$. Following ref. [10.5], we set $\rho_2 = 0$ in what follows. We rewrite this as 4 coupled equations (10.58), and two driven ones for the two angles,

$$\begin{pmatrix} \dot{\theta}_1 \\ \dot{\theta}_2 \end{pmatrix} = \begin{pmatrix} -\sigma \frac{r_1}{r_1} \sin \theta \\ e + (\rho_1 - z) \frac{1}{r_1} \sin \theta \end{pmatrix}. \quad (\text{S.24})$$

Our result confirms formulas stated in ref. [10.5]. (R. Wilczak and P. Cvitanović)

Solution 10.13 - Visualizations of the complex Lorenz flow in polar coordinates. (solution not available)

Solution 10.14 - Computing the relative equilibrium TW_1 . A relative equilibrium point occurs when the derivatives (10.58) are equal to zero (so that the difference between the two angles θ_1 and θ_2 is constant, but the angles themselves are not constant). We use the Solve function (or the Reduce function) in Mathematica to find these points.

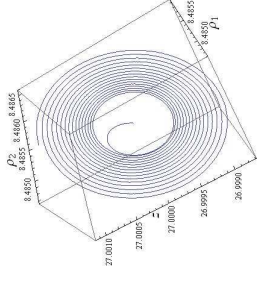


Figure S.9: (r_1, r_2, z) plot of the complex Lorenz flow, with initial point close to TW_1 (note the scales).

We define the system in Solve by setting all time derivatives in (10.58) to zero. Mathematica returns eight solutions of the form

$$\begin{aligned} z(t) &\rightarrow \rho_1 - 1 - \frac{e^2}{(\sigma + 1)^2} \\ r_2(t) &\rightarrow \pm \frac{\sqrt{e^2 + (\sigma + 1)^2} \sqrt{-b(e^2 - (\rho_1 - 1)(\sigma + 1)^2)}}{(\sigma + 1)^2} \\ r_1(t) &\rightarrow \pm \frac{\sqrt{-b(e^2 - (\rho_1 - 1)(\sigma + 1)^2)}}{|\sigma + 1|} \\ \theta(t) &\rightarrow \pm \cos^{-1} \left(\pm \frac{\sqrt{(\sigma + 1)^2}}{\sqrt{e^2 + (\sigma + 1)^2}} \right) \end{aligned} \quad (\text{S.25})$$

The solutions differ by combinations of negative and positive r_1, r_2, θ . A negative r_1 solution corresponds to the same group orbit of solutions, related to the positive r_1 solution by a rotation by π . The $r_1 \geq 0, r_2 \geq 0$ condition in (10.57) reduces these solutions to two, differing by the sign of \cos^{-1} term. As will be further shown in exercise 10.16, the two $\pm \cos^{-1}(\dots)$ solutions are equivalent. We can write the solution compactly as in (10.59), in agreement with ref. [10.5]. For the (10.2) parameter values, the relative equilibrium is at

$$x_{TW_1} = (r_1, r_2, \theta, z) = (8.48527, 8.48562, 0.00909066, 26.9999). \quad (\text{S.26})$$

The angular velocity of relative equilibrium TW_1 follows from (S.24). Both angles move with the same velocity (10.60) and period $T_{TW_1} = 2\pi(\sigma + 1)/\sigma e$. $T_{TW_1} = 69.115 \dots$ for the (10.2) parameter values. That implies that the simulation has to be run up to time of order of at least 70 for the strange attractor in figure 10.1 to start filling in. (R. Wilczak and P. Cvitanović)

Solution 10.15 - Relative equilibrium TW_1 in polar coordinates. The same method as in exercise (10.1) can be used here. First, a numerical solution is found with NDSolve for t going 0 to 10 and initial point TW_1 . We again set MaxSteps \rightarrow Infinity in order to resolve the structure of the flow. Using ParametricPlot3D to plot the flow in (r_1, r_2, z) axes, Figure S.9 illustrates the shape of the flow with (10.2) parameter values. (R. Wilczak)

Solution 10.16 - Relative equilibrium TW_1 in Cartesian coordinates. Using the same method as in exercise 10.15 and in exercise 10.1, we can plot the relative equilibrium in Cartesian coordinates. However, the Cartesian system is five-dimensional

and our polar system has only four dimensions. To resolve this, we set θ_2 to an arbitrary value and set $\theta_1 = \theta + \theta_2$. With this and (10.57), we can verify the numerical value (10.61) of a point on the TW_1 orbit in Cartesian coordinates. Using *Mathematica* to plot the system with t going from 0 to 100, figure 10.4 shows the complex Lorenz flow at TW_1 projected onto the $\{x_1, x_2, z\}$ subspace.

Note that the for a relative equilibrium the flow is along a circle, i.e., the group-orbit of any point on it, but due to finite precision of the initial point and the integration, the trajectory eventually spirals away in a "horn" shape. This circle cuts through the middle of the complex Lorenz equations strange attractor, as shown in figure 10.1. (R. Wilczak)

Solution 10.17 - Eigenvalues and eigenvectors of TW_1 stability matrix. Using the *Mathematica* function *EigenSystem* and setting $(r_1, r_2, \theta, z)(0)$ to the values in (S.26) we obtain

$$(\lambda_{1,2}, \lambda_3, \lambda_4) = (0.0938179 \pm 10.1945i, -11.0009, -13.8534)$$

as the eigenvalues of the system with the associated eigenvectors:

$$\begin{aligned} \operatorname{Re} e_1 &= (0.266121, -0.0321133, 0.00034139, 0.719222) \\ \operatorname{Im} e_1 &= (0.295017, 0.569063, 0.000551886, 0) \\ e_3 &= (-0.0883591, -0.0851485, -0.989135, -0.0809553) \\ e_4 &= (-0.855586, -0.329912, -0.00273531, -0.398902) \end{aligned} \quad (\text{S.27})$$

(R. Wilczak and P. Cvitanović)

Solution 10.18 - The eigen-system of TW_1 stability matrix in polar coordinates. In order to plot the complex eigenvectors, we split them into their real and complex parts as in exercise 10.20. Using the same method as in exercise 10.1, exercise 10.16, and exercise 10.15, we can plot the flow in polar coordinates with an initial point very near to TW_1 along one of the eigenvectors. Figure S.10 shows just this. (R. Wilczak)

Solution 10.19 - Eigenvalues and eigenvectors of EQ_0 stability matrix. Using the *Mathematica* function *EigenSystem* and setting $(x_1, x_2, y_1, y_2, z) = (0, 0, 0, 0, 0)$ at $t = 0$ we obtain the eigenvalues, the associated eigenvectors:

$$\begin{aligned} (\lambda_{1,2}, \lambda_{3,4}, \lambda_5) &= (11.8277 \pm 0.062985i, -22.8277 \pm 0.037015i, -2.66667) \\ e_1 = e_2^* &= (0.00132196 + 0.458131i, 0.458131 - 0.00132196i, i, 1, 0) \\ e_3 = e_4^* &= (0.002249 - 0.779551i, -0.779551 - 0.002249i, 2.84217 + i, 1, 0) \\ e_5 &= (0, 0, 0, 0, 1). \end{aligned} \quad (\text{S.28})$$

(R. Wilczak)

Solution 10.20 - The eigen-system of the stability matrix at EQ_0 . In order to plot the complex eigenvectors, we split them into their real and complex parts and plot each separately (so that one complex eigenvector becomes two, defining a plane). By examining the eigensystem, we can get a sense of what happens to points near the equilibrium EQ_0 . The numerical values of the real parts of the eigenvalues determine

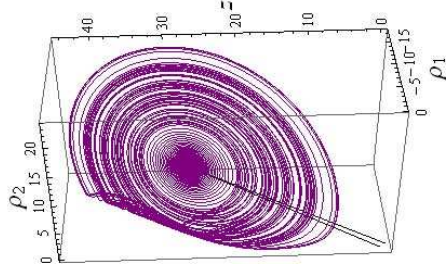


Figure S.10: (r_1, r_2, z) plot of the eigenvector e_3 with initial point at $\frac{1}{100}e_3$ (violet), integrated for time t from 0 to 100.

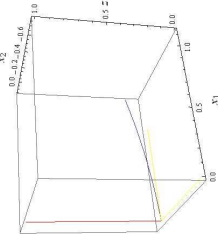


Figure S.11: (x_1, x_2, z) plot of the expanding eigenvector e_1 (red) and the contracting eigenvector e_4 (yellow) of the equilibrium EQ_0 stability matrix of complex Lorenz flow, with initial point at $0.01e_4$.

how quickly the flow will converge onto or diverge away from the equilibrium. For a positive real part the flow will diverge, and for a negative real part it will converge. Complex eigenvalues also indicate that the motion will be spiraling.

For the complex Lorenz equations equilibrium EQ_0 , the values (S.28) of the imaginary parts are orders of magnitude smaller than the real parts, so that there will be very little spiraling. The large values of the real parts tell us that the flow will diverge/converge from the equilibrium very quickly.

To illustrate this, we plot the eigenvectors (as real and imaginary parts) and the flow at initial points close to EQ_0 . The two real vectors (corresponding to a single complex eigenvector) define the plane in which the flow will spiral. We initiate the flow very close to EQ_0 at a point along one of these vectors. In figure S.11, we can see that for the vectors with a very small imaginary part and a positive real part, the flow does not spiral noticeably and that it diverges away from the equilibrium very quickly.

We arrive at figure S.11 using the same method as in the previous plotting exercises (exercise 10.1, exercise 10.15, exercise 10.16). As the eigenvalues are nearly real, the stable/unstable $2d$ manifolds barely spiral, and are not very illuminating. (R.

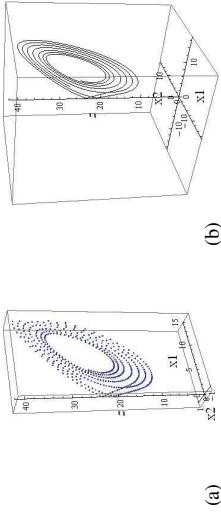


Figure S.12: (a) $\{x_1, x_2, z\}$ plot of the complex Lorenz flow as each point is rotated back to the plane. The time step used to make this plot was 0.01 and the integration went from $t = 0$ to $t = 50$. (b) With the points connected into a curve.

Wilczak

Solution 10.21 - SO(2) or harmonic oscillator slice: We can now construct a moving frame as follows. We write out explicitly the group transformations:

$$\begin{aligned} \bar{x} &= x \cos \theta - y \sin \theta \\ \bar{y} &= x \sin \theta + y \cos \theta. \end{aligned}$$

Then set $\bar{x} = 0$ and solve (S.29) for the group parameter to obtain the moving frame

$$\theta = \tan^{-1} x/y \tag{S.29}$$

which brings any point back to the slice. Substituting (S.29) in the remaining equation, we get the SO(2)-invariant expression $\bar{y} = \sqrt{x^2 + y^2}$.

Solution 10.22 - State space reduction by a slice. We start by setting the initial point and the time step that will be used during the integration. Using Mathematica, we first remove the z component of the initial point so that we have $x(0) \cdot \dot{z} = \{x_1(0), x_2(0), y_1(0), y_2(0), 0\}$. In order to rotate each of the points, we must construct the group representation matrix (10.18), where θ is the angle between the new point (minus the z component) and the positive x_1 axis ($\hat{x}_1 = [1, 0, 0, 0, 0]$). From exercise 10.5, we know that the complex Lorenz equations are invariant for this kind of rotation, so that when we reduce the complex Lorenz flow it contains the same information as the 5-dimensional system. We do not need to determine the angles themselves, we need only their cosines and sines. The cosine is found by a dot product as $\cos(\theta) = x \cdot \hat{x}_1 / |x|$.

Sines can be found by rotating each point by $\pi/2$ and then taking the dot product as with cosine. Taking the first point, we first rotate it with g , and starting with this rotated point, we integrate over the defined time step. We then take the last point from the integration, find its g and rotate it, then use it at the beginning of the next integration from $t = \text{timestep}$ to $t = 2 \cdot \text{timestep}$. This process continues (using a For loop in Mathematica) until the end of the integration (at an arbitrary time). The resulting list of rotated points is then plotted. Using this method, we produced figure S.12. (R. Wilczak)

Solution 10.23 - State space reduction by a slice, ODE formulation: Infinitesimal time version of the moving frames symmetry reduction is attained by taking small time steps in figure 10.11 and dropping the higher order terms, as in sect. 10.4.2:

$$dX^{(t)} = dt v(x^{(t)}) + dt d^{(t)} \mathbf{T} X^{(t)}.$$

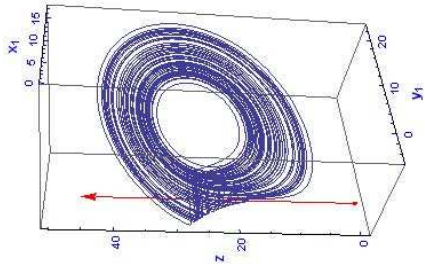


Figure S.13: Method of moving frames, continuous time version, for the polar coordinates motivated $x^* = (0, 1, 0, 0)$, $x_1 = 0$, $x_2 > 0$, slice. The strange attractor of figure 10.1 in the reduced state space, $\{x_2, y_2, z\}$ projection exhibits a discontinuity at $x_2 = 0$.

The infinitesimal angle is proportional to the time step,

$$\theta_1^{(t)} \approx \sin \theta_1^{(t)} = -dt \frac{\hat{e}_1 \cdot v(x^{(t)})}{r_1^{(t)}} \approx -dt v_1(x^{(t)})/x_2^{(t)},$$

where (r_1, θ_1) are polar coordinates, $r_1 = (x_1^2 + x_2^2)^{1/2}$, see (10.57). Our slice condition is $x_1 = 0$, $x_2 > 0$, so the reduced state space equations are given by

$$\dot{x} = v - \frac{v_1}{x_2} \mathbf{T}x. \tag{S.30}$$

The motion stays in the $(d-1)$ -slice, as $\dot{x}_1 = 0$ due to the orthogonal action of \mathbf{T} to the direction x . Moving frames symmetry reduced complex Lorenz equations are a 4-dimensional first order ODE system

$$\begin{aligned} \dot{x}_2 &= -\sigma(x_2 - y_2) \\ \dot{y}_1 &= -y_1 + p_2 x_2 - (e + \sigma y_1/x_2) y_2 \\ \dot{y}_2 &= -y_2 + (p_1 - z) x_2 + (e + \sigma y_1/x_2) y_1 \\ \dot{z} &= -bz + x_2 y_2. \end{aligned} \tag{S.31}$$

The resulting trajectory is illustrated in figure S.13. It agrees with trajectories reported by Siminos (there the simulation is in the full state space, and the reduced state space dynamics is obtained by a coordinate change).

- Checked that it agrees with finite step + rotation of figure 10.11
 - x_2 and y_2 seem locked, oscillate the same way with amplitude up to 20
 - y_1 is very small, mostly below 0.1
 - (x_2, y_2, z) plot looks discontinuous in y_2 whenever x_2 small, across the z -axis (indicated in red).
- Wilczak

Solution 10.24 - Accumulated phase shift in slice reduced state space: (not available)

Solution 10.25 - The moving frame flow stays in the reduced state space: The motion stays in the $(d-1)$ -dimensional slice, as the flow along the group action direction vanishes,

$$\dot{x} \cdot \mathbf{T}y' = v \cdot \mathbf{T}y' - \frac{(v \cdot \mathbf{T}y')}{(x \cdot y')_4} (\mathbf{T}x) \cdot \mathbf{T}y' = 0.$$

(P. Cvitanović)

Solution 10.26 - State space reduction by a relative equilibrium TW , **cross-section.** We note that $x_{TW} \cdot T_{TW} = 0$ by the antisymmetry of \mathbf{T} , so (10.64) is a linear condition $\hat{x} \cdot \mathbf{T}x_{TW} = x \cdot g(\theta)T_{x_{TW}} = 0$ that determines θ . Substituting (10.55) and (10.17) yields a formula

$$\tan \theta = \frac{x_1 x_2^{TW_1} - x_1 x_2^{TW_2} + y_1 y_2^{TW_1} - y_1 y_2^{TW_2}}{x_1 x_1^{TW_1} + x_2 x_2^{TW_1} + y_1 y_1^{TW_1} + y_2 y_2^{TW_1}} \quad (\text{S.32})$$

for the rotation angle $\hat{x} = g(\theta)x$ (actually, there are two solutions, separated by π) that rotates x into the cross-section. In contrast to fixing one of the polar angles as in the method of moving frames of sect. 10.4.1, this cross-section introduces no singularities, as $x_1^2 + x_2^2 + y_1^2 + y_2^2 > 0$. To compute $\sin \theta$, $\cos \theta$ needed by $g(\theta)$ rewrite (S.32) as

$$\begin{aligned} \cos \theta &= (x_1 x_1^{TW_1} + x_2 x_2^{TW_1} + y_1 y_1^{TW_1} + y_2 y_2^{TW_1})/N \\ \sin \theta &= (x_1 x_2^{TW_1} - x_1 x_2^{TW_2} + y_1 y_2^{TW_1} - y_1 y_2^{TW_2})/N, \end{aligned} \quad (\text{S.33})$$

(P. Cvitanović)

with N fixed by $\sin^2 + \cos^2 = 1$.

Chapter 11. Qualitative dynamics, for pedestrians

Solution 11.1 - Binary symbolic dynamics. Read the text.

Solution 11.2 - Generating prime cycles. (No solution available.)

Solution 11.3 - A contracting baker's map. (No solution available.)

Solution 11.4 - Unimodal map symbolic dynamics. Hint: write down an arbitrary binary number such as $\gamma = .1101001101000\dots$ and generate the future itinerary S^+ by checking whether $f^n(\gamma)$ is greater or less than $1/2$. Then verify that (11.9) recovers γ .

Solution 11.4 - Unimodal map symbolic dynamics. The easiest way to see this is to derive the itinerary from the binary expansion using the tent map as the prototypical example of a unimodal map. Let the binary expansion of x be $x = .\omega_1 \omega_2 \omega_3 \omega_4 \dots$ then $1-x = .\bar{\omega}_1 \bar{\omega}_2 \bar{\omega}_3 \bar{\omega}_4 \dots$ with $\bar{\omega} = 1-\omega$. Thus the tent map can be written as

$$T.\omega_1 \omega_2 \omega_3 \dots = \begin{cases} .\omega_2 \omega_3 \omega_4 \dots & \text{if } \omega_1 = 0 \\ .\bar{\omega}_2 \bar{\omega}_3 \bar{\omega}_4 \dots & \text{if } \omega_1 = 1 \end{cases} = \begin{cases} .\omega_2 \omega_3 \omega_4 \dots & \text{if } \omega_1 = 0 \\ 1 - .\omega_2 \omega_3 \omega_4 \dots & \text{if } \omega_1 = 1 \end{cases}$$

Since the symbol of x is simply ω_1 we can generate the symbolic sequence from the binary expansion of x via $s_n = (T^{n-1}x)_1$ for all $n \geq 1$.

Note that $T(1-x) = Tx$ hence for all $n \geq 1$

$$T^n x = T \sigma^{n-1} x = \begin{cases} \sigma^n x & \text{if } (\sigma^{n-1} x)_1 = 0 \\ 1 - \sigma^n x & \text{if } (\sigma^{n-1} x)_1 = 1 \end{cases} = \begin{cases} \sigma^n x & \text{if } \omega_n = 0 \\ 1 - \sigma^n x & \text{if } \omega_n = 1 \end{cases}$$

with σ being the left shift. Therefore, given the symbol sequence s_n we have for $n \geq 1$

$$s_{n+1} = (T^n x)_1 = \begin{cases} (\sigma^n x)_1 & \text{if } \omega_n = 0 \\ (1 - \sigma^n x)_1 & \text{if } \omega_n = 1 \end{cases} = \begin{cases} \omega_{n+1} & \text{if } \omega_n = 0 \\ 1 - \omega_{n+1} & \text{if } \omega_n = 1 \end{cases}$$

which shows

$$\omega_{n+1} = \begin{cases} s_{n+1} & \text{if } \omega_n = 0 \\ 1 - s_{n+1} & \text{if } \omega_n = 1 \end{cases} \quad \text{with } \omega_1 = s_1$$

for all $n \geq 1$.

(Alexander Grigo)

Solution 11.5 - Unimodal map kneading value. (No solution available.)

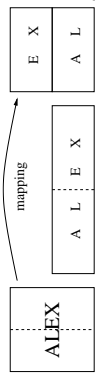
Solution 11.6 - "Golden mean" pruned map.

(a) Consider the 3-cycle drawn in the figure. Denote the lengths of the two horizontal intervals by a and b . We have $a/b = b/(a+b)$, so the slope is given by the golden mean, $\Lambda = b/a = (1 + \sqrt{5})/2$, and the piecewise linear tent map is given by

$$f(x) = \begin{cases} \Lambda x, & x \in [0, 1/2] \\ \Lambda(1-x), & x \in [1/2, 1] \end{cases}$$

Chapter 12. Qualitative dynamics, for cyclists

Solution 12.3 - Slicing Danish without flipping. The action of an orientation preserving baker map is given by



with the right half sliced off and slid over the top of the left half. A formal way of writing the map is

$$T: [0, 1]^2 \rightarrow [0, 1]^2 \text{ with } T(x, y) = \begin{cases} (2x, \frac{1}{2}y) & \text{if } x < \frac{1}{2} \\ (2x - 1, \frac{1}{2}y + \frac{1}{2}) & \text{if } \frac{1}{2} < x \end{cases} \pmod{0}.$$

It is immediate from the figure that a coding is obtained by symbols

$$0 \leftrightarrow \{x < 1/2\} \text{ and } 1 \leftrightarrow \{x > 1/2\}$$

which correspond to the left and right half of the square, respectively. The corresponding symbolic dynamics is indicated in figure S.14, which shows the itineraries for up

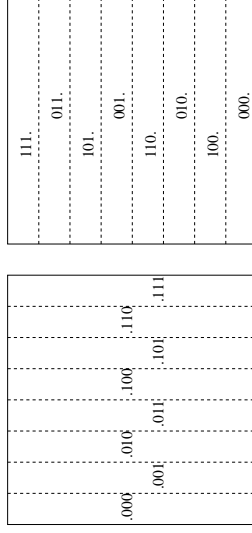


Figure S.14: Itineraries of three steps in forward (left figure) and backward (right figure) direction. The digits on the left of the decimal dot are the past, and the decimal on the right are the future starting with the current symbol.

to three steps in forward and backward direction. The slicing, orientation preserving baker map is simply a 2-dimensional version of the Bernoulli shift map (23.6), with the spatial ordering the same as the temporal ordering. (Alexander Grigo)

Solution 14.1 - Time reversibility. A link between two nodes, say n_1 and n_2 , is present if and only if the map takes some points belonging to symbol n_1 to points with symbol n_2 . Thus for a fine enough partition there will be no symmetry between n_1 to n_2 and $n_2 \rightarrow n_1$. As a simple example consider the rotation by a fixed angle α of the plane around the origin (which is a Hamiltonian map). If α is very small and positive,

Alternative derivation: 3-cycle periodic point at $x = 1/2$ is a fixed point of the 3rd iterate, $f^3(1/2) = \Lambda^2(1 - \Lambda/2) = 1/2$. $\Lambda = 1, (1 - \sqrt{5})/2$ solutions are no good, so $\Lambda = (1 + \sqrt{5})/2$.

(b) The 3-cycle periodic points are $\{x_{C10}, x_{10C}, x_{0C1}\} = \{1/2, \Lambda/2, 1/(2\Lambda)\}$. Once a point enters the region covered by the interval M of length $a + b$, bracketed by the 3-cycle, it will be trapped there forever. Outside M , all points on unit interval will be mapped to $(0, 1/2]$, except for 0. The points in the interval $(0, 1/(2\Lambda))$ approach M monotonically.

(c) It will land in $(\frac{1}{2}, \frac{\Lambda}{2})$.

(d) From (b), we know that except for $x_0 = 0$, all periodic orbits should be in M . By (c), we cannot have the substring 00 in a periodic orbit (except for the fixed point at 0). Hence 00... is the only pruning block, and the symbolic dynamics is a finite subshift, with alphabet $\{0, 1\}$ and only one grammar rule: a consecutive repeat of symbol 0 is inadmissible.

(e) There are two exceptions. 0 is an isolated periodic orbit with itinerary $\bar{0}$. It is unstable and no point in its neighborhood returns to it, and it plays only an indirect role in the asymptotic dynamics. However, the 3-cycle in the figure is important, as it includes the critical point x_c and thus defines the attractor basin boundary. If it is labeled $\bar{010}$ (that is what it becomes if Λ is increased slightly) rather than $\bar{010}$ (here 'C' is the symbol for the critical point), it also violates the 00... pruning rule. (Y. Lan and P. Cvitanović)

Solution 11.7 - Binary 3-step transition matrix. (No solution available.)

Solution 11.8 - Full tent map periodic points. (a) For short cycles it is easy to solve the fixed point condition $(11, 11)$, with

$$f(\gamma) = \begin{cases} f_0(\gamma) = 2\gamma & \text{if } \gamma < 1/2 \\ f_1(\gamma) = 2(1 - \gamma) & \text{if } \gamma > 1/2 \end{cases} \quad (S.34)$$

directly. The 2-cycle periodic points satisfy $f_1 \circ f_0(\gamma_{01}) = 4(1 - \gamma_{01}) = \gamma_{01}$ the 3-cycle periodic points satisfy

$$\begin{aligned} f_1 \circ f_0 \circ f_0(\gamma_{001}) &= 2(1 - 4\gamma_{001}) = \gamma_{001} \\ f_1 \circ f_0 \circ f_0(\gamma_{011}) &= 2(1 - 2(1 - \gamma_{011})) = \gamma_{011}, \end{aligned}$$

etc., yielding periodic points $\{\gamma_{01}, \gamma_{01}\} = \{2/5, 4/5\}$, $\{\gamma_{001}, \gamma_{010}, \gamma_{100}\} = \{2/9, 4/9, 8/9\}$ $\{\gamma_{011}, \gamma_{110}, \gamma_{101}\} = \{2/7, 4/7, 6/7\}$. But this gets tedious quickly, while formula (11.12) is just a formula:

$$(b) \{\gamma_{00111}, \gamma_{01110}, \gamma_{11100}, \gamma_{11001}, \gamma_{10011}\} = \{2/11, 4/11, 8/11, 6/11, 10/11\}.$$

$$(c) \{\gamma_{00001}, \gamma_{00010}, \gamma_{00100}, \gamma_{01000}, \gamma_{10000}\} = \{2/33, 4/33, 8/33, 16/33, 32/33\}.$$

(d)

and if we partition the plane into three equal sectors about the origin, denoted by 1, 2, 3, then the corresponding transition graph has transition matrix

$$M = \begin{pmatrix} 1 & 1 & 0 \\ 0 & 1 & 1 \\ 1 & 0 & 1 \end{pmatrix}$$

which has no symmetry in forward/backward direction, i.e. $M \neq M^T$. Furthermore, the eigenvalues of M are $\Lambda = \{2, \frac{1}{2} \pm \frac{\sqrt{3}}{2}i\}$ hence are not all real.

To see that the transition matrices for Hamiltonian are not necessarily diagonalizable, consider the symplectic mappings of the plane $(x, y) \rightarrow (x, y-1)$ or $(x, y) \rightarrow (2x, y/2)$. Choose two symbols, $1 \leftrightarrow \{y < 0\}$, $2 \leftrightarrow \{y > 0\}$, and $1 \leftrightarrow \{|x| > 1/4\}$, $2 \leftrightarrow \{|x| < 1/4\}$, respectively. Then in both cases the transition matrix reads

$$M = \begin{pmatrix} 1 & 1 \\ 0 & 1 \end{pmatrix}$$

which is not diagonalizable.

(Alexander Grigo)

Chapter 13. Fixed points, and how to get them

Solution 13.1 - Cycles of the Ulam map. Minimizing (see chapter 29)

$$F(x_1, \dots, x_n) = \frac{1}{n} \sum_{i=1}^n [f(x_i) - x_{i+1}]^2$$

using steepest descent

$$\begin{aligned} \nabla F &= \sum_{i=1}^n [f(x_i) - x_{i+1}] [f'(x_i) e_i - e_{i+1}] \\ &= \sum_{i=1}^n [f(x_i) - x_{i+1}] f'(x_i) e_i - \sum_{i=1}^n [f(x_{i-1}) - x_i] e_i \\ &= \sum_{i=1}^n [f(x_i) f'(x_i) - f(x_{i-1}) + x_i - x_{i+1} f'(x_i)] e_i \end{aligned}$$

$$x^{(n+1)} = x^{(n)} - \Delta x_n \frac{F(x^{(n)}) \nabla F(x^{(n)})}{\|\nabla F(x^{(n)})\|^2} \quad \text{with } \Delta x_n \in (0, 1],$$

we can find periodic points of f of period N . The values of the Λ_n are chosen to be the least power of $1/2$ (including the power zero) such that the new point $x^{(n+1)}$ has all coordinates in the unit interval and has the same topological order with respect to the partition $((0, 1/2), (1/2, 1))$ as $x^{(n)}$.

$\frac{p}{0}$	$\frac{x_1}{0.0}$	$\frac{\Lambda}{2}$	$\frac{p}{01}$	$\frac{x_1}{0.3454915028}$	$\frac{x_2}{0.9045084972}$	$\frac{\Lambda}{-4}$
$\frac{1}{1}$	$\frac{1.0}{1.0}$	$\frac{-2}{-2}$				
$\frac{p}{001}$	$\frac{x_1}{0.1169777784}$	$\frac{x_2}{0.4131759111}$	$\frac{x_3}{0.9698463104}$	$\frac{\Lambda}{-8}$		
$\frac{011}{011}$	$\frac{0.188250991}{0.611260467}$	$\frac{x_2}{0.611260467}$	$\frac{x_3}{0.9504844339}$	$\frac{\Lambda}{8}$		
$\frac{p}{0001}$	$\frac{x_1}{0.03376388529}$	$\frac{x_2}{0.1304955414}$	$\frac{x_3}{0.4538658202}$	$\frac{x_4}{0.9974865498}$	$\frac{\Lambda}{-16}$	
$\frac{0011}{0011}$	$\frac{0.04322727119}{0.2771308221}$	$\frac{0.1654346968}{0.8013173182}$	$\frac{0.5522642317}{0.6368314951}$	$\frac{0.9890738004}{0.9251085679}$	$\frac{16}{-16}$	

(Alexander Grigo)

Solution 13.2 - Cycles stabilities for the Ulam map, exact. Since eigenvalues of the monodromy matrix corresponding to any periodic orbit are invariant under (reasonably smooth) change of coordinates we can use the following two observations to prove the claim. Let $U(x)$ denote the Ulam map, and let $T(x)$ denote the tent map.

Firstly, note that the change of variables

$$x' = h(x) = \frac{1}{2} (1 + \sin(\pi(2x - 1))) = \frac{1 - \cos(\pi x)}{2}$$

satisfies

$$h(1 - |x|) = \frac{1 - \cos(\pi(1 - |x|))}{2} = \frac{1 + \cos(\pi|x|)}{2} = 1 - h(|x|) = 1 - h(x)$$

and therefore

$$\begin{aligned} U \circ h(x) &= 4h(x)[1 - h(x)] = [1 + \cos(\pi x)][1 - \cos(\pi x)] = \frac{\sin(\pi x)^2}{1 - \cos(\pi(2x - 1))} \\ h \circ T(x) &\equiv h(1 - 2|x - 1/2|) = 1 - h(2x - 1) = 1 - \frac{2}{1 - \cos(\pi(2x - 1))} \\ &= \frac{1 - \cos(2\pi x)}{2} = \sin(\pi x)^2, \end{aligned}$$

which shows that h conjugates T and U .

Secondly, the tent map $T(x) = 1 - 2|x - 1/2|$ has derivative ± 2 everywhere (except, of course, at $x = 1/2$). The derivative is 2 on the left of $1/2$, i.e. on the symbol 0, and it is -2 on its right, i.e. on the symbol 1. Therefore the periodic orbit with symbolic representation $s_1 s_2 \dots s_N$ has the eigenvalue $\Lambda = (-1)^{\sum_{i=1}^N s_i} 2^N \equiv (-1)^{\#1} 2^N$, as was observed numerically. (Alexander Grigo)

Solution 13.3 - Stability of billiard cycles. The 2-cycle $\bar{0}$ stability (13.7) is the solution to both problems (provided you evaluate correctly the hyperbola curvature on the diagonal).

Solution 13.3 - Stability of billiard cycles. In both cases there is one periodic orbit, the 2-cycle along the shortest line segment connecting the two scatterers. The stability is given by the monodromy matrix

$$J = \begin{bmatrix} -\left(\frac{1}{2} \frac{0}{1}\right) \left(\frac{1}{0} \frac{L}{1}\right)^2 & \left[-\left(\frac{1}{2} \frac{L}{1+2L}\right)\right]^2 \end{bmatrix}$$

with eigenvalues $\Lambda_u = [-(1 + L + \sqrt{2L + L^2})]^2$ and $\Lambda_s = 1/\Lambda_u$.

For the billiard with the straight line and the hyperbola, the monodromy matrix reads

$$\begin{aligned} L &= \sqrt{2} \text{ and } \kappa \text{ hyperbola} = \frac{y'(-1)}{\sqrt{1 + y'(-1)^2}} = \frac{\sqrt{2}}{2} \\ \text{hence } J &= \begin{pmatrix} 1 & 0 \\ 2\kappa & 1 \end{pmatrix} \begin{pmatrix} 1 & 2L \\ 0 & 1 \end{pmatrix} = \begin{pmatrix} 1 & 0 \\ \sqrt{2} & 1 \end{pmatrix} \begin{pmatrix} 1 & 2\sqrt{2} \\ 0 & 1 \end{pmatrix} \\ &= \begin{pmatrix} 1 & 2\sqrt{2} \\ \sqrt{2} & 5 \end{pmatrix} \end{aligned}$$

with eigenvalues $\Lambda_u = 3 + 2\sqrt{2}$ and $\Lambda_s = 1/\Lambda_u$.

(Alexander Grigo)
Solution 13.4 - Numerical cycle routines. A number of sample Fortran programs for finding periodic orbits is available on ChaosBook.org/extras.

Solution 13.13 - Inverse iteration method for a Hamiltonian repeller. For the complete repeller case (all binary sequences are realized), the cycles can be evaluated variationally, as follows. According to (3.19), the coordinates of a periodic orbit of length n_p satisfy the equation

$$x_{p,i+1} + x_{p,i-1} = 1 - a x_{p,i}^2, \quad i = 1, \dots, n_p, \quad (S.35)$$

with the periodic boundary condition $x_{p,0} = x_{p,n_p}$.

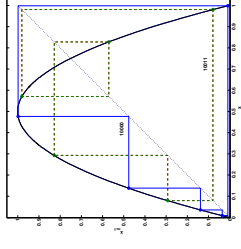
In the complete repeller case, the Hénon map is a realization of the Smale horseshoe, and the symbolic dynamics has a very simple description in terms of the binary alphabet $\epsilon \in \{0, 1\}$, $\epsilon_{p,i} = (1 + S_{p,i})/2$, where $S_{p,i}$ are the signs of the corresponding periodic point coordinates $S_{p,i} = x_{p,i}/|x_{p,i}|$. We start with a preassigned sign sequence $S_{p,1}, S_{p,2}, \dots, S_{p,n_p}$, and a good initial guess for the coordinates $x'_{p,i}$. Using the inverse of the equation (13.26)

$$x'_{p,i} = S_{p,i} \sqrt{\frac{1 - x'_{p,i+1} - x'_{p,i-1}}{a}} \quad i = 1, \dots, n_p$$

we converge iteratively, at exponential rate, to the desired periodic points $x_{p,i}$. Given the periodic points, the cycle stabilities and periods are easily computed using (4.53). The itineraries and the stabilities of the short periodic orbits for the Hénon repeller (S.35) for $a = 6$ are listed in table ??; in actual calculations all prime cycles up to topological length $n = 20$ have been computed. (G. Vattay)

Solution 13.15 - Ulam map periodic points.

- (a) $\{x_{001111}, x_{011110}, x_{111000}, x_{110001}, x_{100111}\} = \{0.079373, 0.292292, 0.827430, 0.571157, 0.979746\}$
- (b) $\{x_{00001}, x_{00010}, x_{00100}, x_{01000}, x_{10000}\} = \{0.009036, 0.0355816, 0.138132, 0.476209, 0.997736\}$
- (c)



D. Borrero

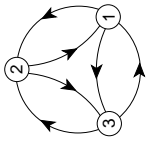
Chapter 14. Walkabout: Transition graphs

Solution 14.1 - Time reversibility** The answer is "no." Work out a few simple Hamiltonian maps as counterexamples.

Solution 14.2 - Alphabet {0,1}; prune $_11000 \rightarrow _001100 \rightarrow _011100 \rightarrow$. This is worked out in the exercise itself.

Chapter 15. Counting

Solution 15.1 - A transition matrix for 3-disk pinball. a) As the disk is convex, the transition to itself is forbidden. Therefore, the transition graph is



with the corresponding transition matrix

$$T = \begin{pmatrix} 0 & 1 & 1 \\ 1 & 0 & 1 \\ 1 & 1 & 0 \end{pmatrix}.$$

Note that $T^2 = T + 2$. Suppose that $T^n = a_n T + b_n$, then

$$T^{n+1} = a_n T^2 + b_n T = (a_n + b_n)T + 2a_n.$$

So $a_{n+1} = a_n + b_n$, $b_{n+1} = 2a_n$ with $a_1 = 1$, $b_1 = 0$.

b) From a) we have $a_{n+1} = a_n + 2a_{n-1}$. Suppose that $a_n \propto \lambda^n$. Then $\lambda^2 = \lambda + 2$. Solving this equation and using the initial condition for $n = 1$, we obtain the general formula

$$a_n = \frac{1}{3}(2^n - (-1)^n),$$

$$b_n = \frac{2}{3}(2^n + (-1)^n).$$

c) T has eigenvalues $\{2, -1, -1\}$. So the topological entropy is $\ln 2$, the same as in the case of the binary symbolic dynamics.

Solution 15.3 - Sum of A_{ij} is like a trace. Suppose that $A\phi_k = \lambda_k\phi_k$, where λ_k, ϕ_k are eigenvalues and eigenvectors, respectively. Expressing the vector $v = (1, 1, \dots, 1)^T$ in terms of the eigenvectors ϕ_k , i.e., $v = \sum_k d_k \phi_k$, we have

$$\Gamma_n = \sum_{ij} [A^n]_{ij} = v^T A^n v = \sum_k v^T A^n d_k \phi_k = \sum_k d_k \lambda_k^n (v^T \phi_k)$$

$$= \sum_k c_k \lambda_k^n,$$

where $c_k = (v^T \phi_k) d_k$ are constants.

a) As $\text{tr} A^n = \sum_k \lambda_k^n$, it is easy to see that both $\text{tr} A^n$ and Γ_n are dominated by the largest eigenvalue λ_0 . That is

$$\frac{\ln |\text{tr} A^n|}{\ln |\Gamma_n|} = \frac{n \ln |\lambda_0| + \ln |\sum_k (\frac{\lambda_k}{\lambda_0})^n|}{n \ln |\lambda_0| + \ln |\sum_k d_k (\frac{\lambda_k}{\lambda_0})^n|} \rightarrow 1 \text{ as } n \rightarrow \infty.$$

b) The nonleading eigenvalues do not need to be distinct, as the ratio in a) is controlled by the largest eigenvalues only. (Y. Lan)

Solution 15.5 - Transition matrix and cycle counting. a) According to the definition of \mathbb{T}_{ij}^n , the transition matrix is

$$\mathbb{T} = \begin{pmatrix} a & c \\ b & 0 \end{pmatrix}.$$

b) All walks of length three 0000, 0001, 0010, 0100, 0101, 1000, 1001, 1010 (four symbols!) with weights $aaa, aac, atc, cba, cbc, baa, bac, bcb$. Let's calculate \mathbb{T}^3 ,

$$\mathbb{T}^3 = \begin{pmatrix} a^3 + 2abc & a^2c + bc^2 \\ a^2b + b^2c & abc \end{pmatrix}.$$

There are altogether 8 terms, corresponding exactly to the terms in all the walks.

c) Let's look at the following equality

$$\mathbb{T}_{ij}^n = \sum_{k_1, k_2, \dots, k_{n-1}} \mathbb{T}_{ik_1} \mathbb{T}_{k_1 k_2} \dots \mathbb{T}_{k_{n-1} j}.$$

Every term in the sum is a possible path from i to j , though the weight could be zero. The summation is over all possible intermediate points ($n - 1$ of them). So, \mathbb{T}_{ij}^n gives the total weight (probability or number) of all the walks from i to j in n steps.

d) We take $a = b = c = 1$ to just count the number of possible walks in n steps. This is the crudest description of the dynamics. Taking a, b, c as transition probabilities would give a more detailed description. The eigenvalues of \mathbb{T} is $(1 \pm \sqrt{5})/2$, so we get $N(n) \propto (\frac{1+\sqrt{5}}{2})^n$.

e) The topological entropy is then $\ln \frac{1+\sqrt{5}}{2}$.
Solution 15.7 - "Golden mean" pruned map. It is easy to write the transition matrix \mathbb{T}

$$\mathbb{T} = \begin{pmatrix} 0 & 1 \\ 1 & 1 \end{pmatrix}.$$

The eigenvalues are $(1 \pm \sqrt{5})/2$. The number of periodic orbits of length n is the trace

$$\mathbb{T}^n = \frac{(1 + \sqrt{5})^n + (1 - \sqrt{5})^n}{2^n}.$$

(Y. Lan)
Solution 15.2 - 3-disk prime cycle counting. The formula for arbitrary length cycles is derived in sect. 15.4.

Solution 15.10 - Whence Möbius function? Written out $f^{(n)}$ line-by-line for a few values of n , (15.43) yields

$$\begin{aligned} f(1) &= g(1) \\ f(2) &= g(2) + g(1) \\ f(3) &= g(3) + g(1) \\ f(4) &= g(4) + g(2) + g(1) \\ &\dots \\ f(6) &= g(6) + g(3) + g(2) + g(1) \\ &\dots \end{aligned} \tag{S.36}$$

Now invert recursively this infinite tower of equations to obtain

$$\begin{aligned} g(1) &= f(1) \\ g(2) &= f(2) - f(1) \\ g(3) &= f(3) - f(1) \\ g(4) &= f(4) - [f(2) - f(1)] - f(1) = f(4) - f(2) \\ &\dots \\ g(6) &= f(6) - [f(3) - f(1)] - [f(2) - f(1)] - f(1) \\ &\dots \end{aligned}$$

We see that $f^{(n)}$ contributes with factor -1 if n prime, and not at all if n contains a prime factor to a higher power. This is precisely the raison d'être for the Möbius function, with whose help the inverse of (15.43) can be written as the Möbius inversion formula [27.29] (15.44).

Solution 15.16 - Alphabet (a, b, c), prune .ab.. This pruning rule implies that any string of "b's" must be preceded by a "c," so one possible alphabet is (a, cb^k, \bar{b}) , $k=0, 1, 2, \dots$. As the rule does not prune the fixed point \bar{b} , it is explicitly included in the list. The cycle expansion (15.15) becomes

$$\begin{aligned} 1/\zeta &= (1 - t_a)(1 - t_b)(1 - t_c) \times \\ &= (1 - t_{cb})(1 - t_{ac})(1 - t_{abb}) \dots \\ &= 1 - t_a - t_b - t_c + t_{ab} - (t_{cb} - t_c t_b) \\ &\quad - (t_{ac} - t_a t_c) - (t_{abb} - t_{ab} t_b) \dots \end{aligned}$$

The effect of pruning $.ab..$ is to unbalance the 2-cycle curvature $t_{cb} - t_c t_b$; the remainder of the cycle expansion retains the curvature form.

Solution 15.18 - Alphabet (0, 1), prune .1000., .00100., .01100.,

step 1. .1000. prunes all cycles with a .000. subsequence with the exception of the fixed point 0; hence we factor out $(1 - t_0)$ explicitly, and prune .000. from the rest. Physically this means that x_0 is an isolated fixed point - no cycle stays in its vicinity for more than 2 iterations. In the notation of exercise 15.17, the alphabet is $(1, 2, 3, 0)$, and the remaining pruning rules have to be rewritten in terms of symbols $2=10, 3=100$:

step 2. alphabet $\{1, 2, 3, \bar{0}\}$, prune $\underline{33}$, $\underline{213}$, $\underline{313}$. Physically, the 3-cycle $\bar{3} = \underline{100}$ is pruned and no long cycles stay close enough to it for a single $\underline{100}$. repeat. As in exercise 15.6, prohibition of $\underline{33}$ is implemented by dropping the symbol "3" and extending the alphabet by the allowed blocks $\underline{13}$, $\underline{23}$.

step 3. alphabet $\{1, 2, \underline{13}, \underline{23}, \bar{0}\}$, prune $\underline{213}$, $\underline{2313}$, $\underline{1313}$, where $\underline{13} = \underline{13}$, $\underline{23} = \underline{23}$ are now used as single letters. Pruning of the repetitions $\underline{1313}$, $\underline{1313}$ (the 4-cycle $\underline{13} = \underline{1100}$ is pruned) yields the

Result: alphabet $\{1, 2, \underline{23}, \underline{113}, \bar{0}\}$, unrestricted 4-ary dynamics. The other remaining possible blocks $\underline{213}$, $\underline{2313}$ are forbidden by the rules of step 3. The topological zeta function is given by

$$1/\zeta = (1 - t_0)(1 - t_1 - t_2 - t_{23} - t_{113}) \tag{S.37}$$

for unrestricted 4-letter alphabet $\{1, 2, \underline{23}, \underline{113}\}$.

Chapter 16. Transporting densities

Solution 16.1 - Integrating over Dirac delta functions. (a) Whenever $h(x)$ crosses 0 with a nonzero velocity ($\det \partial_x h(x) \neq 0$), the delta function contributes to the integral. Let $x_0 \in h^{-1}(0)$. Consider a small neighborhood V_0 of x_0 so that $h : V_0 \rightarrow V_0$ is a one-to-one map, with the inverse function $x = x(h)$. By changing variable from x to h , we have

$$\begin{aligned} \int_{V_0} dx \delta(h(x)) &= \int_{h(V_0)} dh |\det \partial_{h,x}| \delta(h) = \int_{h(V_0)} dh \frac{1}{|\det \partial_x h|} \delta(h) \\ &= \frac{1}{|\det \partial_x h|_{h=0}}. \end{aligned}$$

Here, the absolute value $|\cdot|$ is taken because delta function is always positive and we keep the orientation of the volume when the change of variables is made. Therefore all the contributions from each point in $h^{-1}(0)$ add up to the integral

$$\int_{\mathbb{R}^d} dx \delta(h(x)) = \sum_{x \in h^{-1}(0)} \frac{1}{|\det \partial_x h|}.$$

Note that if $\det \partial_x h = 0$, then the delta function integral is not well defined.

(b) The formal expression can be written as the limit

$$F := \int_{\mathbb{R}} dx \delta(x^2) = \lim_{\sigma \rightarrow 0} \int_{\mathbb{R}} dx \frac{e^{-x^2/\sigma}}{\sqrt{2\pi\sigma}},$$

by invoking the approximation given in the exercise. The change of variable $y = x^2/\sqrt{\sigma}$ gives

$$F = \lim_{\sigma \rightarrow 0} \sigma^{-3/4} \int_{\mathbb{R}^+} dy \frac{e^{-y^2}}{\sqrt{2\pi y}} = \infty,$$

where \mathbb{R}^+ represents the positive part of the real axis. So, the formal expression does not make sense. The zero derivative of x^2 at $x = 0$ invalidates the expression in (a). (Y. Lan)

Solution 16.2 - Derivatives of Dirac delta functions. We do this problem just by direct evaluation. We denote by Ω_y a sufficiently small neighborhood of y . (a)

$$\begin{aligned} \int_{\mathbb{R}} dx \delta'(y) &= \sum_{x \in y^{-1}(0)} \int_{\Omega_y} dy \det \left(\frac{dy}{dx} \right)^{-1} \delta'(y) \\ &= \sum_{x \in y^{-1}(0)} \frac{\delta'(y)}{|y'|} \Big|_{x=y} - \int_{\Omega_y} dy \frac{\delta(y)}{y^2} (-y') \frac{1}{y'} \\ &= \sum_{x \in y^{-1}(0)} \frac{y''}{|y'| y^2}, \end{aligned}$$

where the absolute value is taken to take care of the sign of the volume.

$$\begin{aligned}
(b) \quad \int_{\mathbb{R}} dx \delta^{(2)}(y) &= \sum_{x \in \mathbb{S}^{-1}(0)} \int_{\Omega_x} dy \frac{\delta^{(2)}(y)}{y'} \\
&= \sum_{x \in \mathbb{S}^{-1}(0)} \frac{\delta'(y)}{|y'|} \Big|_{y=\epsilon} - \int_{\Omega_x} dy \frac{\delta'(y)}{y^2} (-y') \frac{1}{y'} \\
&= \sum_{x \in \mathbb{S}^{-1}(0)} \frac{y'' \delta(y)}{|y'| y'^2} \Big|_{y=\epsilon} - \int_{\Omega_x} dy \delta(y) \frac{d}{dx} \left(\frac{y''}{y^3} \right) \frac{1}{y'} \\
&= \sum_{x \in \mathbb{S}^{-1}(0)} - \int_{\Omega_x} dy \delta(y) \left(\frac{y'''}{y^3} - 3 \frac{y''^2}{y^4} \right) \frac{1}{y'} \\
&= \sum_{x \in \mathbb{S}^{-1}(0)} \left(3 \frac{y''^2}{y^4} - \frac{y'''}{y^3} \right) \frac{1}{|y'|}.
\end{aligned}$$

$$\begin{aligned}
(c) \quad \int_{\mathbb{R}} dx b(x) \delta^{(2)}(y) &= \sum_{x \in \mathbb{S}^{-1}(0)} \int_{\Omega_x} dy b(x) \frac{\delta^{(2)}(y)}{y'} \\
&= \sum_{x \in \mathbb{S}^{-1}(0)} \frac{b(x) \delta'(y)}{|y'|} \Big|_{y=\epsilon} - \int_{\Omega_x} dy \delta'(y) \frac{d}{dx} \left(\frac{b}{y'} \right) \frac{1}{y'} \\
&= \sum_{x \in \mathbb{S}^{-1}(0)} -\delta(y) \frac{d}{dx} \left(\frac{b}{y'} \right) \frac{1}{y'} \Big|_{y=\epsilon} + \int_{\Omega_x} dy \delta(y) \frac{d}{dx} \left(\frac{b}{y'} \right) \frac{1}{y'} \\
&= \sum_{x \in \mathbb{S}^{-1}(0)} \frac{1}{|y'|} \frac{d}{dx} \left(\frac{b y''}{y^3} - \frac{b y'''}{y^3} \right) \\
&= \sum_{x \in \mathbb{S}^{-1}(0)} \frac{1}{|y'|} \left[\frac{b y''}{y^3} - \frac{b' y''}{y^3} - 2 \frac{b y'''}{y^4} + b \left(3 \frac{y''^2}{y^4} - \frac{y'''}{y^3} \right) \right] \\
&= \sum_{x \in \mathbb{S}^{-1}(0)} \frac{1}{|y'|} \left(\frac{b y''}{y^3} - 3 \frac{b' y''}{y^4} + b \left(3 \frac{y''^2}{y^4} - \frac{y'''}{y^3} \right) \right).
\end{aligned}$$

Solution 16.3 - \mathcal{L}^1 generates a semigroup. Every "sufficiently good" transformation f^t in state space \mathcal{M} is associated with a Perron-Frobenius operator \mathcal{L}^t which is when acting on a function $\rho(x)$ in \mathcal{M}

$$\mathcal{L}^t \cdot \rho(x) = \int_{\mathcal{M}} dy \delta(x - f^t(y)) \rho(y).$$

In some proper function space \mathcal{F} on \mathcal{M} , the one parameter family of operators $\{\mathcal{L}^t\}_{t \in \mathbb{R}^+}$ generate a semigroup. Let's check this statement. For any $t_1, t_2 > 0$ and $\rho \in \mathcal{F}$, the product "o" of two operators is defined as usual

$$(\mathcal{L}^{t_1} \circ \mathcal{L}^{t_2}) \cdot \rho(y) = \mathcal{L}^{t_1} \cdot (\mathcal{L}^{t_2} \cdot \rho)(y).$$

So, we have

$$(\mathcal{L}^{t_1} \circ \mathcal{L}^{t_2})(y, x) = \int_{\mathcal{M}} dz \mathcal{L}^{t_1}(y, z) \mathcal{L}^{t_2}(z, x)$$

$$\begin{aligned}
&= \int_{\mathcal{M}} dz \delta(y - f^{t_1}(z)) \delta(z - f^{t_2}(x)) \\
&= \delta(y - f^{t_1}(f^{t_2}(x))) \\
&= \delta(y - f^{t_1+t_2}(x)) \\
&= \mathcal{L}^{t_1+t_2}(y, x),
\end{aligned}$$

where the semigroup property $f^{t_1}(f^{t_2}(x)) = f^{t_1+t_2}(x)$ of f^t has been used. This proves the claim in the title. (Y. Lan)

Solution 16.5 - Invariant measure. Hint: We do (a),(b),(c),(d) for the first map and (e) for the second.

(a) The partition point is in the middle of $[0, 1]$. If the density on the two pieces are two constants ρ_0^A and ρ_0^B , respectively, the Perron-Frobenius operator still leads to the piecewise constant density

$$\rho^A = \frac{1}{2}(\rho_0^A + \rho_0^B), \quad \rho^B = \frac{1}{2}(\rho_0^A + \rho_0^B).$$

In general, if a finite Markov partition exists and the map is linear on each partition cell, a finite-dimensional invariant subspace which is a piecewise constant function can always be identified in the function space.

(b) From the discussion of (a), any constant function on $[0, 1]$ is an invariant measure. If we consider the invariant probability measure, then the constant has to be 1.

(c) As the map is invariant in $[0, 1]$ (there is no escaping), the leading eigenvalue of \mathcal{L} is always 1 due to the "mass" conservation.

(d) Take a typical point on $[0, 1]$ and record its trajectory under the first map for some time (10^5 steps). Plot the histogram... ONLY 0 is left finally! This happens because of the finite accuracy of the computer arithmetics. A small trick is to change the slope 2 to 1.99999999. You will find a constant measure on $[0, 1]$ which is the natural measure. Still, the finite precision of the computer will make every point eventually periodic and strictly speaking the measure is defined only on subsets of lattice points. But as the resolution improves, the computer-generated measure steadily approaches the natural measure. For the first map, any small deviation from the constant profile will be stretched and smeared out. So, the natural measure has to be constant.

(e) Simple calculation shows that α is the partition point. We may use A, B to mark the left and right part of the partition, respectively. A maps to B and B maps to the whole interval $[0, 1]$. As the magnitude of the slope $\Lambda = (\sqrt{5} + 1)/2$ is greater than 1, we may expect the natural measure is still piecewise constant with eigenvalue 1. The determining equation is

$$\begin{pmatrix} 0 & 1/\Lambda \\ 1/\Lambda & 1/\Lambda \end{pmatrix} \begin{pmatrix} \rho^A \\ \rho^B \end{pmatrix} = \begin{pmatrix} \rho^A \\ \rho^B \end{pmatrix},$$

which gives $\rho^B / \rho^A = \Lambda$.

For the second map, the construction of Exercise 15.7 is worth a look. (Y. Lan)

Chapter 17. Averaging

Solution 17.1 - How unstable is the Hénon attractor?

1. Evaluate numerically the Lyapunov exponent by iterating the Hénon map: For $a = 1.4$, $b = 0.3$ the answer should be close to $\lambda = 0.41922\dots$. If you have a good estimate and a plot of the convergence of your estimate with n , please send us your results for possible inclusion into this text.

2. Both Lyapunov exponents for $a = 1.39945219$, $b = 0.3$ are negative, roughly $\lambda_1 = -0.2712$, $\lambda_2 = -0.9328$ (check that these values respect the constant volume contraction condition (4.54) for the Hénon map). Why? Because after a long transient exploration of the Hénon map's non-wandering set, on average after some 11,000 iterates, almost every initial point falls into a stable 13-cycle. You can check its existence by starting at one of its periodic points $(x_p, y_p) = (-0.2061, -0.3181)$.

If you missed the stable 13-cycle (as all students in one of the courses did), you should treat your computer experiments with great deal of scepticism.

As the product of eigenvalues is the constant $-b$, you need to evaluate only the expanding eigenvalue. There are many ways to implement this calculation - here are a few:

1. The most naive way - take the log of distance of two nearby trajectories, iterate until you run out of accuracy. Try this many times, estimate an average.
2. Slightly smarter: as above, but keep rescaling the length of the vector connecting neighboring points so it remains small, average over the sum of logs of rescaling factors. You can run this forever.
3. Keep multiplying the $[2 \times 2]$ Jacobian stability matrix (4.53) until you run out of accuracy. Compute the log of the leading eigenvalue - try this many times, estimate an average.
4. Slightly smarter still: as above, but start with an arbitrary initial tangent space vector, keep multiplying it with the Jacobian stability matrix, and rescaling the length of the vector so it remains small. You can run this forever.
5. There is probably no need to use the QR decomposition method or any other such numerical method for this 2-dimensional problem.

(Y. Lan and P. Cvitanović)
Solution 17.4 - Rössler attractor Lyapunov exponents. J. Sprott: $(\lambda_1, \lambda_2, \lambda_3) = (0.0714, 0, -5.3943)$

Solution 16.4 - The escape rate is the leading zero of the zeta function

$$0 = 1/\zeta(\gamma) = 1 - e^{-\gamma}/2a - e^{-\gamma}/2a = 1 - e^{-\gamma}/a.$$

So, $\gamma = \log(a)$ if $a > a_c = 1$ and $\gamma = 0$ otherwise. For $a \approx a_c$ the escape rate behaves like

$$\gamma(a) \approx (a - a_c).$$

Solution 16.7 - Eigenvalues of the skew full tent map Perron-Frobenius operator.

If we have density $\rho_N(x)$, the action of the Perron-Frobenius operator associated with $f(x)$ gives a new density

$$\rho_{N+1}(x) = \frac{1}{\Lambda_0} \rho_N(x/\Lambda_0) + \frac{1}{\Lambda_1} \rho_N(1 - x/\Lambda_1),$$

where $\Lambda_i = \frac{dN}{dN+1}$. The eigenvalue equation is given by

$$\rho_{N+1}(x) = \lambda \rho_N(x). \tag{S.38}$$

We may solve it by assuming that the eigenfunctions are N -th order polynomials $P(N)$ (check it). Indeed, detailed calculation gives the following results:

- $P(0)$ gives $\lambda = 1$, corresponding to the expected leading eigenvalue.
- $P(1)$ gives $\lambda = \frac{1}{\Lambda_0} - \frac{1}{\Lambda_1} = \frac{2}{\Lambda_0} - 1$,
- $P(2)$ gives $\lambda = \frac{1}{\Lambda_0} + \frac{1}{\Lambda_1}$,
- $P(3)$ gives $\lambda = \frac{1}{\Lambda_0} - \frac{1}{\Lambda_1}$,
- The guess is that $P(N)$ gives $\lambda = \frac{1}{\Lambda_0^N} + (-1)^N \frac{1}{\Lambda_1^N}$.

The final solution is that the piecewise linear function $\rho^A = -\Lambda_0, \rho^B = \Lambda_1$ gives the eigenvalue 0. If only the continuous functions are considered, this kind of eigenfunction of course should not be included.

(Y. Lan)

Solution 16.7 - Eigenvalues of the skew full tent map Perron-Frobenius operator.

$$e^{s_0} = 1, \quad e^{s_1} = \frac{2}{\Lambda_0} - 1$$

$$e^{s_2} = \frac{1}{4} + \frac{3}{4} \left(\frac{2}{\Lambda_0} - 1 \right)^2, \quad e^{s_3} = \frac{1}{2} \left(\frac{2}{\Lambda_0} - 1 \right) + \frac{1}{2} \left(\frac{2}{\Lambda_0} - 1 \right)^3 \dots$$

For eigenvectors (invariant densities for skew tent maps), see for example L. Billings and E.M. Bolt [16.14].

Solution 16.10 - \mathcal{A} as a generator of translations.

If v is a constant in space, Taylor series expansion gives

$$a(x + n) = \sum_{k=0}^{\infty} \frac{1}{k!} (v \frac{\partial}{\partial x})^k a(x) = e^{n \frac{v}{a}} a(x).$$

(Y. Lan)

Chapter 18. Trace formulas

(No solutions available.)

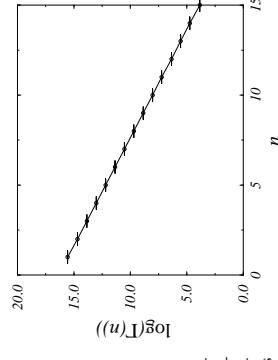


Figure S.15: Plot of $\log(\Gamma(n))$ versus n for the logistic map $x_{n+1} = 6x_n(1-x_n)$. Error bars show estimated errors in the mean assuming a binomial distribution. 10,000,000 random initial starting points were used.

Chapter 19. Spectral determinants

Solution 19.1 - Numerical estimate of the escape rate for a 1-dimensional repeller
The logistic map is defined by $x_{n+1} = Ax_n(1-x_n)$. For $A \leq 4$ any point in the unit interval $[0, 1]$ will remain in the interval forever. For $A > 4$ almost all points starting in the unit interval will eventually escape towards $-\infty$.

The rate of escape can be easily measured by numerical experiment. We define the fraction of initial conditions that leave the interval after n iterations to be Γ_n . Figure S.15 shows a plot of $\log(\Gamma_n)$ versus n , computed by starting with 10,000,000 random initial points. Asymptotically the escape rate falls off exponentially as

$$\Gamma(n) = Ce^{-\gamma n}.$$

Figure S.15 suggests that this formula is very accurate even for relatively small n . We estimate γ by measuring the slope of the curve in figure S.15. To avoid errors due to rounding and transients only the points $5 \leq n \leq 10$ were used. A linear regression fit yields the escape rate for $A = 6$:

$$\gamma = 0.8315 \pm 0.0001,$$

where the error is from statistical fluctuations (there may be systematic errors either due to rounding or because we are not in the true asymptotic regime).

(Adam Prügel-Bennet)

Solution 19.3 - Dynamical zeta functions

1. Work through section sect. 19.3.2.
2. Generalize the transition matrix (14.10) to a transfer operator.

Solution 19.2 - Spectrum of the “golden mean” pruned map.

1. The idea is that with the redefinition $2 = 10$, the alphabet $\{1, 2\}$ is unrestricted binary, and due to the piecewise linearity of the map, the stability weights factor in a way similar to (18.11).

2. As in (19.9), the spectral determinant for the Perron-Frobenius operator takes form (19.11)

$$\det(1 - z\mathcal{L}) = \prod_{k=0}^{\infty} \frac{1}{\zeta_k}, \quad \frac{1}{\zeta_k} = \prod_p \left(1 - \frac{z^{d_p}}{|\Lambda_p| \Lambda_p^k} \right).$$

The mapping is piecewise linear, so the form of the topological zeta function worked out in (15.19) already suggests the form of the answer. The alphabet (1.2) is unrestricted binary, so the dynamical zeta functions receive contributions only from the two fixed points, with all other cycle contributions cancelled exactly. The $1/\zeta_0$ is the spectral determinant for the transfer operator like the one in (17.19) with the $T_{00} = 0$, and in general

$$\begin{aligned} \frac{1}{\zeta_k} &= \left(1 - \frac{z}{|\Lambda_1| \Lambda_1^k} \right) \left(1 - \frac{z^2}{|\Lambda_2| \Lambda_2^k} \right) \left(1 - \frac{z^3}{|\Lambda_{12}| \Lambda_{12}^k} \right) \dots \\ &= 1 - (-1)^k \left(\frac{z}{\Lambda^{k+1}} + \frac{z^2}{\Lambda^{2k+2}} \right). \end{aligned} \quad (\text{S.39})$$

The factor $(-1)^k$ arises because both stabilities Λ_1 and Λ_2 include a factor $-\Lambda$ from the right branch of the map.

Solution 19.6 - Dynamical zeta functions as ratios of spectral determinants. Try inserting a factor equal to one in the zeta function and then expanding it. The problem is solved in sect. 19.5.

Solution 19.9 - Dynamical zeta functions for Hamiltonian maps. Read example 19.7.

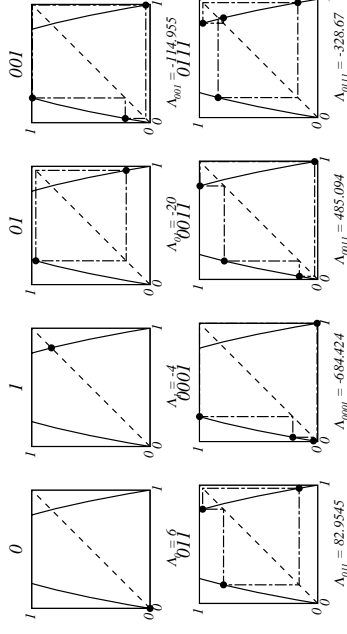


Figure S.16: Periodic orbits and stabilities for the logistic equation $x_{n+1} = \delta x_n(1 - x_n)$.

Chapter 20. Cycle expansions

Solution 20.2 - Prime cycles for a 1-dimensional repeller, analytic formulas. For the logistic map the prime cycles, ordered in terms of their symbolic dynamics, are listed in table 15.1

$$\mathbf{P} = \{0, 1, 01, 001, 011, 0001, 0011, 0111, \dots\}$$

The position of the prime cycles can be found by iterating the inverse mapping. If we wish to find the position of a prime orbit $p = b_1 b_2 \dots b_{|p|}$, where $b_i \in \{0, 1\}$, then starting from some initial point, $x = 1/2$ say, we apply one of the inverse mappings

$$f_{\pm}^{-1}(x) = \frac{1}{2} \pm \frac{1}{2} \sqrt{1 - x/4A}$$

where we choose f_{-}^{-1} if $b_1 = 0$ or f_{+}^{-1} if $b_1 = 1$. We then apply the inverse mapping again depending on the next element in the prime orbit. Repeating this procedure many times we converge onto the prime cycle. The stability Λ_p of a prime cycle p is given by the product of slopes of f around the cycle. The first eight prime cycles are shown in figure S.16.

The stabilities of the first five prime orbits can be calculated for arbitrary A . We find that $\Lambda_0 = A$, $\Lambda_1 = 2 - A$, $\Lambda_{01} = 4 + 2A - A^2$, and

$$\Lambda_{011} = 8 + 2A - A^2 \pm A(2 - A) \sqrt{A^2 - 2A - 7}. \quad (\text{S.40})$$

There is probably a closed form expression for the 4-cycles as well.

For crosschecking purposes: if $A = 9/2$, $\Lambda_0 = 9/2$, $\Lambda_1 = -5/2$, $\Lambda_{01} = -7.25$, $\Lambda_{011} = 19.942461 \dots$

(Adam Prügel-Bennet)

Solution 20.2 - Dynamical zeta function for a 1-dimensional repeller The escape rate can be estimated from the leading zero in the dynamical zeta function $1/\zeta(z)$, defined by

$$1/\zeta(z) = \prod_p \left(1 - z^{\tau_p}/|\Lambda_p|\right).$$

To compute the position of this pole we expand $1/\zeta(z)$ as a power series (20.7) in z

$$1/\zeta(z) = 1 - \sum_{i=1}^n \hat{c}_i z^i$$

where

$$\hat{c}_1 = |\Lambda_0|^{-1} + |\Lambda_1|^{-1}, \quad \hat{c}_2 = |\Lambda_{00}|^{-1} - |\Lambda_1 \Lambda_0|^{-1}$$

$$\hat{c}_3 = |\Lambda_{000}|^{-1} - |\Lambda_{00} \Lambda_{01}|^{-1} + |\Lambda_{011}|^{-1} - |\Lambda_{01} \Lambda_1|^{-1}$$

etc.. Using the cycles up to length 6 we get

$$1/\zeta(z) = 1 - 0.416667z - 0.0083333z^2 + 0.000079446z^3 - 9.89291 \times 10^{-7}z^4 + \dots$$

The leading zero of this Taylor series is an estimate of $\exp(\gamma)$. Using $n = 1, 2, 3$ and 4 we obtain the increasingly accurate estimates for γ : 0.875469, 0.830597, 0.831519 and 0.831492 in a hope to improve the convergence we can use the Padé approximates $P_N^M(z) = \sum_{i=1}^N P_i z^i / (1 + \sum_{j=1}^M Q_j z^j)$. Using the Padé approximates $P_1^{-1}(z)$ for $n = 2, 3$ and 4 we obtain the estimates 0.828585, 0.831499 and 0.831493.

The above results correspond to $A = 6$; in the $A = 9/2$ case the leading zero is $1/z = 1.43549 \dots$ and $\gamma = 0.36150 \dots$ (Adam Prügel-Bennet)

Solution 20.2 - Spectral determinant for a 1-dimensional repeller We are told the correct expression for the escape rate is also given by the logarithm of the leading zero of the spectral determinant (19.11), expanded as the Taylor series (20.11). The coefficients c_i should fall off super-exponentially so that truncating the Taylor series is expected to give a far more accurate estimate of the escape rate than using the dynamical zeta function. How do we compute the c_i coefficients in (20.11)? One straightforward method is to first compute the Taylor expansion of $\log(F(z))$

$$\log(F(z)) = \sum_p \sum_{k=0}^{f_p} \log\left(1 - \frac{f_p}{\Lambda_p^k}\right) = - \sum_p \sum_{k=0}^{f_p} \sum_{r=1}^{\infty} \frac{\Lambda_p^{kr}}{k r}$$

$$= - \sum_p \sum_{r=1}^{\infty} \frac{f_p}{1 - \Lambda_p^r} = - \sum_p \sum_{r=1}^{\infty} B_p(r) z^{p r}$$

where $B_p(r) = -1/r(\Lambda_p^r(1 + \Lambda_p^r))$. Writing $\log(F(z))$ as a power series

$$\log(F(z)) = - \sum_{i=1}^n b_i z^i$$

(Adam Prügel-Bennet)

The above results correspond to $A = 6$; in the $A = 9/2$ case all cycles up to length 10 yield $\gamma = 0.36150966984250926 \dots$ (Vadim Moroz)

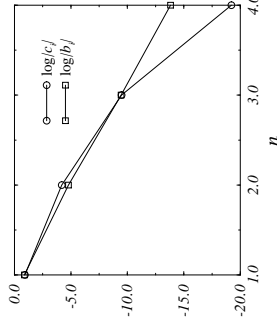


Figure S.17: Plot of the Taylor coefficients for the spectral determinant, c_i , and for the dynamical zeta function, b_i .

we obtain

$$b_1 = B_0(1) + B_1(1)$$

$$b_2 = B_0(1) + B_0(2) + B_1(2)$$

$$b_3 = B_0(1) + B_0(3) + B_1(3)$$

$$b_4 = B_0(1) + B_0(4) + B_1(4) + B_0(2) + B_1(4) + B_1(4) \quad (\text{S.41})$$

etc.. To obtain the coefficients for the spectral determinant we solve

$$F(z) = 1 - \sum_{i=1}^n Q_i z^i = \exp\left(\sum_{i=1}^n b_i z^i\right)$$

for the Q_i 's. This gives

$$Q_1 = b_1, \quad Q_2 = b_2 + b_1^2/2, \quad Q_3 = b_3 + b_1 b_2 + b_1^3/6$$

$$Q_4 = b_4 + b_1 b_3 + b_2^2/2 + b_2 b_1^2/2 + b_1^4/24$$

Using these formulas we find

$$F(z) = 1 - 0.4z - 0.0152381z^2 - 0.0000759784z^3 + 4.5311 \times 10^{-9}z^4 + \dots$$

The logarithm of the leading zero of $F(z)$ again gives the escape rate. Using the $n = 1, 2, 3$, and 4 truncations we find the approximation to γ of 0.916291, 0.832346, 0.83149289 and 0.8314929875. As predicted, the convergence is much faster for the spectral determinant than for the dynamical zeta function.

In figure S.17 we show a plot of the logarithm of the coefficients for the spectral determinant and for the dynamical zeta function.

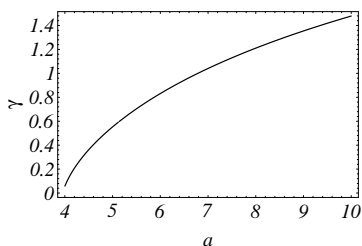


Figure S.18: Plot of the escape rate versus a for the logistic map $x_{n+1} = ax_n(1 - x_n)$ calculated from the first five periodic orbits.

Solution 20.2 - Escape rate for a 1 - dimensional repeller We can compute an approximate functional dependence of the escape rate on the parameter a using the stabilities of the first five prime orbits computed above, see (S.40). The spectral determinant (for $a > 4$) is

$$F = 1 - \frac{2z}{a-1} - \frac{8z^2}{(a-3)(a-1)^2(a+1)} + \left(\frac{2(32 - 18a + 17a^2 - 16a^3 + 14a^4 - 6a^5 + a^6)}{(a-3)(a-1)^3(1+a)(a^2 - 5a + 7)(a^2 + a + 1)} - \frac{2a(a-2)\sqrt{(a^2 - 2a - 7)}}{(a^2 - 5a + 7)(a^2 - 2a - 7)(a^2 + a + 1)} \right) z^3 \quad (\text{S.42})$$

The leading zero is plotted in figure S.18; it always remains real while the other two roots which are large and negative for $a > 5.13 \dots$ become imaginary below this critical value. The accuracy of this truncation is clearly worst for $a \rightarrow 4$, the value at which the hyperbolicity is lost and the escape rate goes to zero.

(Adam Prügel-Bennet)

Solution 20.3 - Escape rate for the Ulam map. The answer is worked out in Nonlinearity 3, 325; 3, 361 (1990).

Solution 20.11 - Escape rate for the Rössler system. No solution available as yet.

Chapter 21. Discrete symmetries factorize spectral determinants.

Solution 21.2 - Sawtooth map desymmetrization. No solution available as yet.

Solution 21.4 - 3-disk desymmetrization.

- b) The shortest cycle with no symmetries is $\overline{121213}$.
- c) The shortest fundamental domain cycle whose time reversal is not obtained by a discrete symmetry is 010011 . It corresponds to $\overline{121313212323}$ in the full space.

Ben Web

Solution 21.5 - C_2 factorizations: the Lorenz and Ising systems. No solution available as yet.

Solution 21.6 - Ising model. No solution available as yet.

Solution 21.7 - One orbit contribution. No solution available as yet.

Solution ?? - Characters. No solution available as yet.

Chapter 22. Why cycle?

Solution 22.1 - The escape is controlled by the size of the primary gap of the repeller. All subgaps in the repeller will be proportional to the main gap. The size of the main gap is $l = \sqrt{1 - 1/a}$. Near $a_c = 1$ the escape rate is

$$\gamma(a) \sim (a - a_c)^{1/2}.$$

We can generalize this and the previous result and conclude that

$$\gamma(a) \sim (a - a_c)^{1/2},$$

where z is the order of the maximum of the single humped map.

Solution 22.2 - By direct evaluation we can calculate the zeta functions and the Fredholm determinant of this map.

$$(a) \quad s_{10} = \frac{\Lambda_0}{\Lambda_0 - 1} \frac{b-1}{b}, \quad s_{10} = -\frac{\Lambda_1 - 1}{\Lambda_1} \frac{b}{b-1}, \quad c = b + \frac{b-1}{\Lambda_1}.$$

(b) Show that the 2-cycle Floquet multiplier does not depend on b ,

$$\Lambda_{01} = s_{01} s_{10} = -\frac{\Lambda_0 \Lambda_1}{(\Lambda_0 - 1)(\Lambda_1 + 1)}.$$

$$(c) \quad \mathbf{L} = \begin{pmatrix} L_{00} & L_{01} \\ L_{10} & L_{11} \end{pmatrix},$$

where $L_{00} = 1/\Lambda_0$, $L_{01} = 1/s_{01}$, $L_{11} = 1/\Lambda_1$, $L_{10} = 1/s_{10}$ are inverses of the slopes of the map.

(e) $\det(1 - z\mathbf{L}) = 1 - ???$

(h) Yes.

The Fredholm determinant is the product of zeta functions

$$F(z) = \prod_{k=0}^{\infty} 1/\zeta_k(z).$$

The leading zeroes of the Fredholm determinant can come from the zeroes of the leading zeta functions.

The zeroes of $1/\zeta_0(z)$ are

$$1/z_1 = \frac{T_{00} + T_{11} + \sqrt{(T_{00} - T_{11})^2 + 4T_0 T_{10}}}{2},$$

$$1/z_2 = \frac{T_{00} + T_{11} - \sqrt{(T_{00} - T_{11})^2 + 4T_0 T_{10}}}{2}.$$

The zeroes of $1/\zeta_1(z)$ are

$$1/z_3 = \frac{T_{00}^2 + T_{11}^2 + \sqrt{(T_{00}^2 - T_{11}^2)^2 + 4T_0^2 T_{10}^2}}{2},$$

$$1/z_4 = \frac{T_{00}^2 + T_{11}^2 - \sqrt{(T_{00}^2 - T_{11}^2)^2 + 4T_0^2 T_{10}^2}}{2}.$$

By substituting the slopes we can show that $z_1 = 1$ is the leading eigenvalue. The next to leading eigenvalue, which is the correlation decay in discrete time, can be $1/z_3$ or $1/z_2$.

Solution 22.3 -

(d) In the $A = 9/2$ case all cycles up to length 9 yield $\lambda = 1.08569 \dots$ (Vadim Moroz)

Chapter 23. Why does it work?

Solution 23.3 - Euler formula. Let

$$P = \prod_{k=0}^{\infty} (1 + u^k) = \sum_{n=0}^{\infty} P_n u^n$$

then

$$P_n = \frac{1}{n!} \left. \frac{\partial^n P}{\partial u^n} \right|_{u=0} = \frac{1}{n!} \sum_{i_0 + i_1 + \dots + i_{n-1} = n} u^{i_0 + i_1 + \dots + i_{n-1}} \quad (\text{S.43})$$

$$= \sum_{i_0 + i_1 + \dots + i_{n-1} \geq 0} u^{i_0 + i_1 + \dots + i_{n-1}}$$

Clearly $P_0 = 1$, and

$$P_1 = \sum_{i=0}^{\infty} u^i$$

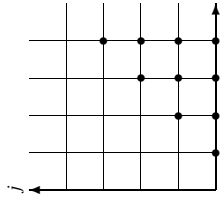
multiplying both sides by $1 - u$

$$(1 - u)P_1 = 1 + u + u^2 + \dots = (u + u^2 + \dots) = 1$$

(since, for $|u| < 1$, $\lim_{n \rightarrow \infty} u^n = 0$). Thus $P_1 = 1/(1 - u)$. Similarly

$$P_2 = \sum_{i>j \geq 0} u^{i+j}$$

Graphically the allowed values of i and j are



Performing the same trick as for P_1

$$(1 - u)P_2 = \sum_{i>j \geq 0} u^{i+j} - \sum_{i \geq j \geq 0} u^{i+(j+1)}$$

The only terms that survive are those for which $j = i - 1$ (that is the top diagonal in the figure) thus

$$(1 - u)P_2 = u^{-1} \sum_{i=1}^{\infty} u^{2i}$$

and

$$(1 - u)(1 - u^2)P_2 = u^{-1} (u^2 + u^4 + \dots + (u^4 + u^6 + \dots)) = u$$

Thus

$$P_2 = \frac{u}{(1 - u)(1 - u^2)}$$

In general

$$(1 - u)P_n = \sum_{i_n > i_{n-1} > \dots > i_1 \geq 0} u^{i_n + i_{n-1} + \dots + i_1} - \sum_{i_n > i_{n-1} > \dots > i_1 \geq 0} u^{i_n + i_{n-1} + \dots + (i_1 + 1)} \quad (\text{S.44})$$

$$= u^{-1} \sum_{i_n > i_{n-1} > \dots > i_2 \geq 1} u^{i_n + i_{n-1} + \dots + 2i_2} \quad (\text{S.45})$$

since only the term $i_1 = i_2 - 1$ survives. Repeating this trick

$$(1 - u)(1 - u^2)P_n = u^{-1-2} \sum_{i_n > i_{n-1} > \dots > i_3 \geq 2} u^{i_n + i_{n-1} + \dots + 3i_3}$$

and

$$\prod_{i=1}^n (1 - u^i) P_n = u^{-(1+2+\dots+n)} u^{n(n-1)} = u^{n(n-1)/2}$$

Thus

$$P_n = \frac{u^{n(n-1)/2}}{\prod_{i=1}^n (1 - u^i)}$$

(Adam Prügél-Bennet)

Solution 23.3 - Euler formula, 2nd method. The coefficients Q_k in (23.4) are given explicitly by the Euler formula

$$Q_k = \frac{1}{1 - \Lambda^{-1}} \frac{\Lambda^{-1}}{1 - \Lambda^{-2}} \dots \frac{\Lambda^{-k+1}}{1 - \Lambda^{-k}} \quad (\text{S.46})$$

Such a formula is easily proved by considering the finite order product

$$\mathcal{W}_j(z, \gamma) = \prod_{l=0}^j (1 + z\gamma^l) = \sum_{l=0}^{j+1} \Gamma_l z^l$$

Since we have that

$$(1 + z\gamma^{j+1})\mathcal{W}_j(z, \gamma) = (1 + z)\mathcal{W}_j(\gamma z, \gamma),$$

we get the following identity for the coefficients

$$\Gamma_m + \Gamma_{m-1}\gamma^{j+1} = \Gamma_m\gamma^m + \Gamma_{m-1}\gamma^{m-1} \quad m = 1, \dots$$

Starting with $\Gamma_0 = 1$, we recursively get

$$\Gamma_1 = \frac{1 - \gamma^{j+1}}{1 - \gamma} \quad \Gamma_2 = \frac{(1 - \gamma^{j+1})(\gamma - \gamma^{j+1})}{(1 - \gamma)(1 - \gamma^2)} \dots$$

the Euler formula (23.5) follows once we take the $j \rightarrow \infty$ limit for $|\gamma| < 1$.

(Robert Artuso)

Solution 23.3 - Euler formula, 3rd method. First define

$$f(t, u) := \prod_{k=0}^{\infty} (1 + tu^k) \quad (\text{S.47})$$

Note that

$$f(t, u) = (1 + t)f(tu, u), \quad (\text{S.48})$$

by factoring out the first term in the product. Now make the ansatz

$$f(t, u) = \sum_{n=0}^{\infty} t^n g_n(u), \quad (\text{S.49})$$

plug it into (S.48), compare the coefficients of t^n and get

$$g_n(u) = u^n g_n(u) + u^{n-1} g_{n-1}(u) \quad (\text{S.50})$$

Of course $g_0(u) = 1$. Therefore by solving the recursion (S.50) and by noting that $\sum_{k=1}^{n-1} k = \frac{n(n-1)}{2}$ one finally arrives at

$$g_n(u) = \frac{u^{\frac{n(n-1)}{2}}}{\prod_{k=1}^n (1 - u^k)} \quad (\text{S.51})$$

Euler got this formula and he and Jacobi got many nice number theoretical results from it, most prominent the pentagonal number theorem, which says that in the series expansion of $\prod_{k=1}^{\infty} (1 - q^k)$ all terms cancel except those which have as an exponent the circumference of a regular pentagon with integer base length.

(Juri Rolf)

Solution 23.4 - 2 - dimensional product expansion. Now let us try to apply the same trick as above to the two dimensional situation

$$h(t, u) := \prod_{k=0}^{\infty} (1 + tu^k)^{k+1}. \quad (\text{S.52})$$

Write down the first terms and note that similar to (S.48)

$$h(t, u) = f(t, u)h(tu, u), \quad (\text{S.53})$$

where f is the Euler product (S.47). Now make the ansatz

$$h(t, u) = \sum_{n=0}^{\infty} t^n a_n(u) \quad (\text{S.54})$$

and use the series expansion for f in (S.53) to get the recursion

$$a_n(u) = \frac{1}{1 - tu^n} \sum_{m=0}^{n-1} u^m a_m(u) g_{n-m}(u). \quad (\text{S.55})$$

With this one can at least compute the generalized Euler product effectively, but it would be nice if one could use it for a proof of the general behaviour of the coefficients a_n .

(Juri Rolf)

Chapter K. Thermodynamic formalism

Solution K.1 - In the higher dimensional case there is no change in the derivation except Λ_p should be replaced with the product of expanding eigenvalues $\prod_j |\Lambda_{p,j}|$. The logarithm of this product is $\sum_j \log |\Lambda_{p,j}|$. The average of $\log |\Lambda_{p,j}|$ is the j th Lyapunov exponent.

(G. Vattay)

Solution K.4 - The zeta function for the two scale map is

$$1/\zeta(z, \beta) = 1 - z \left(\frac{1}{a^\beta} + \frac{1}{b^\beta} \right).$$

The pressure function is

$$P(\beta) = \log z_0(\beta) = -\log \left(\frac{1}{a^\beta} + \frac{1}{b^\beta} \right).$$

The escape rate is

$$\gamma = P(1) = -\log \left(\frac{1}{a} + \frac{1}{b} \right).$$

The topological entropy is

$$K_0 = h_{\text{top}} = -P(0) = \log 2.$$

The Lyapunov exponent is

$$\bar{\lambda} = P'(1) = \frac{\log a/a + \log b/b}{1/a + 1/b}.$$

The Kolmogorov entropy is

$$K_1 = \bar{\lambda} - \gamma = P'(1) - P(1) = \frac{\log a/a + \log b/b}{1/a + 1/b} + \log \left(\frac{1}{a} + \frac{1}{b} \right).$$

The Rényi entropies are

$$K_\beta = (P(\beta) - \beta\gamma)/(\beta - 1) = \left(\log \left(\frac{1}{a^\beta} + \frac{1}{b^\beta} \right) + \beta \log \left(\frac{1}{a} + \frac{1}{b} \right) \right) / (\beta - 1).$$

The box counting dimension is the solution of the implicit equation $P(D_0) = 0$, which is

$$1 = \frac{1}{a^{D_0}} + \frac{1}{b^{D_0}}.$$

The information dimension is

$$D_1 = 1 - \gamma/\bar{\lambda}.$$

The rest of the dimensions can be determined from equation $P(q - (q - 1)D_q) = \gamma q$. Taking exp of both sides we get

$$\frac{1}{a^{q-(q-1)D_q} + b^{q-(q-1)D_q}} = \left(\frac{1}{a} + \frac{1}{b} \right)^q.$$

For a given q we can find D_q from this implicit equation.

Solution ?? - The zeta function is

$$1/\zeta(z, \beta) = \det(1 - \mathbf{T}^{\beta-1}),$$

where we replaced k with $\beta - 1$ in solution S. The pressure can be calculated from the leading zero which is (see solution S)

$$P(\beta) = \log z_0(\beta) = -\log \left(\frac{T_{00}^\beta + T_{11}^\beta + \sqrt{(T_{00}^\beta - T_{11}^\beta)^2 + 4T_{01}^\beta T_{10}^\beta}}{2} \right).$$

Solution K.5 - We can easily read off that $b = 1/2$, $a_1 = \arcsin(1/2)/2\pi$ and $a_2 = a_1$ and do the steps as before.

Chapter 24. Intermittency

(No solutions available.)

yielding $D = 1/3$, in agreement with in (25.21) for $\Lambda = 3$.

Solution 25.6 - Accelerated diffusion. SUGGESTED STEPS

1. Show that the condition assuring that a trajectory indexed by (ϕ, α) hits the (m, n) disk (all other disks being transparent) is written as

$$\left| \frac{d_{m,n}}{R} \sin(\phi - \alpha - \theta_{m,n}) + \sin \alpha \right| \leq 1 \tag{S.57}$$

where $d_{m,n} = \sqrt{n^2 + n^2}$ and $\theta_{m,n} = \arctan(n/m)$. You can then use a small R expansion of (S.57).

2. Now call J_n the portion of the state space leading to a first collision with disk $(n, 1)$ (take into account screening by disks $(1, 0)$ or $(n - 1, 1)$). Denote by $J_n = \bigcup_{k=n+1}^{\infty} J_k$ and show that $J_n \sim 1/n^2$, from which the result for the distribution function follows.

Chapter 28. Noise

Solution 28.2 - d -dimensional Gaussian integrals. We require that the matrix in the exponent is nondegenerate (i.e. has no zero eigenvalues.) The converse may happen when doing stationary phase approximations which requires going beyond the Gaussian saddle point approximation, typically to the Airy-function type stationary points [32.10]. We also assume that M is positive-definite, otherwise the integral is infinite.

Make a change of variables $y = Ax$ such that $A^T M^{-1} A = \text{Id}$. Then

$$I = \frac{1}{(2\pi)^{d/2}} \int_{\mathbb{R}^d} \exp\left(-\frac{1}{2} \sum_{i=1}^d (y_i)^2 - 2(JA)_i y_i\right) |\det A| dy$$

Complete each term under in the sum in the exponent to a full square

$$y_i^2 - 2(JA)_i y_i = (y_i - (JA)_i)^2 - (JA)_i^2$$

and shift the origin of integration to $JA/2$, so that

$$I = \frac{1}{(2\pi)^{d/2}} \exp\left[\frac{1}{2} J^T A A^T J\right] |\det A| \int_{\mathbb{R}^d} \exp\left[-\frac{1}{2} \sum_{i=1}^d y_i^2\right] dy$$

Note that $A A^T M^{-1} A A^T = A A^T$, therefore $A A^T = M$ and $|\det A| = \sqrt{|\det M|}$. The remaining integral is equal to a Poisson integral raised to the d -th power, i.e. $(2\pi)^{d/2}$.
Answer:

$$I = \sqrt{|\det M|} \exp\left[\frac{1}{2} J^T M J\right]$$

(R. Paškauskas)

Chapter 26. Turbulence?

(No solutions available.)

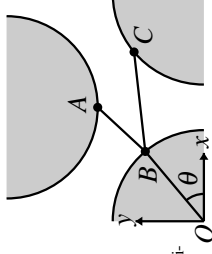


Figure S.20: Minimizing the path from the previous bounce to the next bounce.

Chapter 29. Relaxation for cyclists

Solution 29.1 - Evaluation of cycles by minimization. To start with a guess path where each bounce is given some arbitrary position on the correct disk and then iteratively improve on the guess. To accomplish this an improvement cycle is constructed whereby each bouncing point in the orbit is taken in turn and placed in a new position so that it minimizes the path. Since the positions of all the other bounces are kept constant this involves choosing the new bounce position which minimizes the path from the previous bounce to the next bounce. This problem is schematically represented in figure S.20

Finding the point B involves a one dimensional minimization. We define the vectors $\vec{A} = O\vec{A}$, $\vec{B} = O\vec{B}$ and $\vec{C} = O\vec{C}$. We wish to minimize the length L_{ABC} by varying \vec{B} subject to the constraint that $|\vec{B}| = a$. Clearly

$$\begin{aligned} L_{ABC} &= |\vec{A} - \vec{B}| + |\vec{C} - \vec{B}| \\ &= \sqrt{\vec{A}^2 + \vec{B}^2 - 2\vec{A} \cdot \vec{B}} + \sqrt{\vec{C}^2 + \vec{B}^2 - 2\vec{C} \cdot \vec{B}} \end{aligned}$$

writing

$$\vec{B}(\theta) = a(\cos \theta, \sin \theta)$$

then the minima is given by

$$\frac{dL_{ABC}}{d\theta} = - \left(\frac{\vec{A}}{\sqrt{\vec{A}^2 + \vec{B}^2 - 2\vec{A} \cdot \vec{B}}} + \frac{\vec{C}}{\sqrt{\vec{C}^2 + \vec{B}^2 - 2\vec{C} \cdot \vec{B}}} \right) \cdot \vec{B}'(\theta) = 0.$$

The minima can then be found using a bisection algorithm or using Newton-Raphson. A simpler way is to observe that $\vec{B}'(\theta)$ is orthogonal to $\vec{B}(\theta)$ so that the vector

$$\vec{D} = \frac{\vec{A}}{\sqrt{\vec{A}^2 + \vec{B}^2 - 2\vec{A} \cdot \vec{B}}} + \frac{\vec{C}}{\sqrt{\vec{C}^2 + \vec{B}^2 - 2\vec{C} \cdot \vec{B}}}$$

will be proportional to \vec{B} . This then provides an iterative sequence for finding \vec{B}

- Starting from your current guess for \vec{B} calculate \vec{D}

Chapter 27. Irrationally winding

- Put $\tilde{b} = a\tilde{d}/|\tilde{d}|$
- Repeat the first step until you converge.

At each iteration of the improvement cycle the total length of the orbit is measured. The minimization is complete when the path length stops improving. Although this algorithm is not as fast as the Newton-Raphson method, it nevertheless converges very rapidly.

(No solutions available.)

(Adam Prügel-Bennet)

Chapter 31. Quantum mechanics, briefly

Solution 31.1 - Lorentzian representation of the Dirac delta function. General hint: read up on principal parts, positive and negative frequency parts of the Dirac delta function, perhaps the Cauchy theorem, in any good quantum mechanics textbook.

To see that (31.19) satisfies properties of the delta function,

$$\delta(E - E_n) = -\lim_{\varepsilon \rightarrow 0} \frac{1}{\pi} \operatorname{Im} \frac{1}{E - E_n + i\varepsilon},$$

start by expressing explicitly the imaginary part:

$$\begin{aligned} -\operatorname{Im} \frac{1}{E - E_n + i\varepsilon} &= -\operatorname{Im} \frac{E - E_n - i\varepsilon}{(E - E_n + i\varepsilon)(E - E_n - i\varepsilon)} \\ &= \frac{\varepsilon}{(E - E_n)^2 + \varepsilon^2}. \end{aligned}$$

This is a Lorentzian of width ε , with a peak at $E = E_n$. It has the correct normalization for the delta function,

$$\begin{aligned} \frac{1}{\pi} \int_{-\infty}^{\infty} dE \frac{\varepsilon}{(E - E_n)^2 + \varepsilon^2} &= \frac{1}{\pi} \frac{\varepsilon}{\varepsilon} \arctan \frac{E - E_n}{\varepsilon} \Big|_{-\infty}^{\infty} \\ &= \frac{1}{\pi} (\pi/2 - (-\pi/2)) = 1, \end{aligned}$$

so

$$\frac{1}{\pi} \int_{-\infty}^{\infty} dE \frac{\varepsilon}{(E - E_n)^2 + \varepsilon^2} = 1, \quad (\text{S.58})$$

independently of the width ε .

Next we show that in the $\varepsilon \rightarrow \infty$ limit the support of the Lorentzian is concentrated at $E = E_n$. When $E = E_n$,

$$\lim_{\varepsilon \rightarrow 0} \frac{1}{\pi} \left(\frac{\varepsilon}{(E - E_n)^2 + \varepsilon^2} \right) = \lim_{\varepsilon \rightarrow 0} \frac{1}{\pi} \frac{1}{\varepsilon} = \infty,$$

and when $E \neq E_n$,

$$\lim_{\varepsilon \rightarrow 0} \frac{1}{\pi} \frac{\varepsilon}{(E - E_n)^2 + \varepsilon^2} = 0$$

Providing that a function convolved with $\delta(\varepsilon)$, $\int f(E) \delta(E - E_n) dE$ has a continuous first derivative at $E = E_n$, and falls off sufficiently rapidly as $E \rightarrow \pm\infty$, this is a representation of the delta function.

Solution 31.2 - Green's function. The Laplace transform of the (time-dependent) quantum propagator

$$K(q, q', t) = \sum_n \phi_n(q) e^{-iE_n t/\hbar} \phi_n^*(q')$$

is the (energy-dependent) Green's function

$$\begin{aligned} G(q, q', E + i\varepsilon) &= \frac{1}{i\hbar} \int_0^{\infty} dt e^{\frac{i}{\hbar}(E - \varepsilon)t} \sum_n \phi_n(q) e^{-iE_n t/\hbar} \phi_n^*(q') \\ &= \frac{1}{i\hbar} \sum_n \phi_n(q) \phi_n^*(q') \int_0^{\infty} dt e^{\frac{i}{\hbar}(E - E_n + i\varepsilon)t} \\ &= - \sum_n \phi_n(q) \phi_n^*(q') \frac{1}{E - E_n + i\varepsilon} \Big|_{t=0}^{t=\infty}. \end{aligned}$$

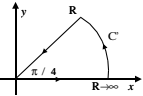
When ε is positive, $e^{-\frac{\varepsilon}{\hbar}t} = 0$, so

$$G(q, q', E + i\varepsilon) = \sum_n \frac{\phi_n(q) \phi_n^*(q')}{E - E_n + i\varepsilon}. \quad (\text{Bo Li})$$

Chapter 32. WKB quantization

Solution 32.1 - Fresnel integral. Start by re-expressing the integral over the infinite half-line:

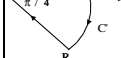
$$\frac{1}{\sqrt{2\pi}} \int_{-\infty}^{\infty} dx e^{-\frac{z^2}{2ia}} = \frac{2}{\sqrt{2\pi}} \int_0^{\infty} dx e^{-\frac{z^2}{2ia}}, \quad a \in \mathbb{R}, \quad a \neq 0.$$

When $a > 0$, the contour  vanishes, as it contains no pole:

$$\begin{aligned} \oint_C dz e^{-z^2/2ia} &= \int_0^{\infty} dx e^{-\frac{z^2}{2ia}} + \int_C + \int_{\infty}^0 e^{i\frac{\pi}{4}} e^{-\frac{z^2}{2ia}} dx = 0 \\ \int_C &= \int_0^{\frac{\pi}{4}} e^{iR^2 e^{2\phi}/2a} R e^{i\phi} i d\phi = 0. \end{aligned} \quad (\text{S.59})$$

So

$$\frac{2}{\sqrt{2\pi}} \int_0^{\infty} dx e^{-\frac{z^2}{2ia}} = \frac{2}{\sqrt{2\pi}} \int_0^{\infty} dx e^{i\frac{\pi}{4}} e^{-\frac{z^2}{2ia}} = e^{i\frac{\pi}{4}} \sqrt{a} = \sqrt{ia}$$

In the $a < 0$ case take the contour 

$$\begin{aligned} \oint_C dz e^{-z^2/2ia} &= \int_0^{\infty} dx e^{-\frac{z^2}{2ia}} + \int_C + \int_{\infty}^0 e^{-i\frac{\pi}{4}} e^{-\frac{z^2}{2ia}} dx \\ &= \int_0^{\infty} dx e^{-\frac{z^2}{2ia}} - e^{-i\frac{\pi}{4}} \int_0^{\infty} dx e^{-\frac{z^2}{2ia}} = 0. \end{aligned}$$

Again

$$\frac{2}{\sqrt{2\pi}} \int_0^{\infty} dx e^{-\frac{z^2}{2ia}} = e^{-i\frac{\pi}{4}} \sqrt{|a|},$$

and, as one should have perhaps intuited by analyticity arguments, for either sign of a we have the same Gaussian integral formula

$$\frac{1}{\sqrt{2\pi}} \int_{-\infty}^{\infty} dx e^{-\frac{z^2}{2ia}} = |a|^{1/2} e^{i\frac{\pi}{4} \frac{a}{|a|}} = \sqrt{ia}.$$

The vanishing of the C' contour segment (S.59) can be proven as follows: Substitute $z = R e^{i\phi}$ into the integral

$$I_R = \int_0^{\frac{\pi}{4}} e^{iR^2 e^{2\phi}/2a} R e^{i\phi} i d\phi = \int_0^{\frac{\pi}{4}} e^{iR^2 (\cos 2\phi + i \sin 2\phi)/2a} R e^{i\phi} i d\phi.$$

Then

$$|I_R| \leq R \int_0^{\frac{\pi}{4}} e^{-R^2 \sin 2\phi/2a} d\phi = \frac{R}{2} \int_0^{\frac{\pi}{2}} e^{-R^2 \sin \theta/2a} d\theta.$$

In the range $[0, \pi/2]$ we can replace $\frac{2}{\pi} \theta \leq \sin \theta$, obtain a bound

$$|I_R| \leq \frac{R}{2} \int_0^{\frac{\pi}{2}} e^{-R^2 \theta/\pi a} d\theta = \frac{R}{2} \frac{1 - e^{-R^2/2a}}{R^2/a\pi},$$

so

$$\lim_{R \rightarrow \infty} |I_R| = 0.$$

(Bo Li)

Chapter 33. Semiclassical evolution

Solution 33.5 - Free particle R-function. Calculate R from its definition

$$R(q', q, t) = \int_0^t \mathcal{L}(\dot{q}(t'), q(t'), t') dt'$$

where the solution of Lagrange equations of motion is substituted for $q(t)$.

a a D -dimensional free particle:

We have

$$\begin{aligned} \mathcal{L}(\dot{q}(t'), q(t'), t') &= \frac{m}{2} \sum_{i=1}^D [\dot{q}_i(t')]^2, \\ \dot{q}_i(t) &= \text{const} = \frac{q'_i - q_i}{t}. \end{aligned} \quad (\text{S.60})$$

The answer:

$$R(q', q, t) = \frac{m}{2} \sum_{i=1}^D \frac{[q'_i - q_i]^2}{t}.$$

b Using symmetric gauge for vector potential and denoting the Larmor frequency by $\omega = \frac{eB}{mc}$, we have

$$\mathcal{L} = \frac{m}{2} (\dot{x}^2 + \dot{y}^2 + \dot{z}^2 + \omega(x\dot{y} - y\dot{x}))$$

The equations of motion are

$$\ddot{x} - \omega\dot{y} = 0, \quad \ddot{y} + \omega\dot{x} = 0, \quad \ddot{z} = 0.$$

To calculate the expression for the principal function we do integration by parts on $\dot{x}^2 + \dot{y}^2$, and the result is

$$R = \int \mathcal{L} dt = \frac{m}{2} \left(x\dot{x}|_{t_0}^t + y\dot{y}|_{t_0}^t + \frac{(z' - z)^2}{t} + \int_{t_0}^t [x(-\ddot{x} + \omega\dot{y}) + y(-\ddot{y} - \omega\dot{x})] dt \right),$$

however terms inside the integral vanish by equations of motion. Denote $w(t) = x(t) + iy(t)$, then the first two equations of motion are equivalent to equation in complex $w(t)$:

$$\dot{w}(t) + i\omega w(t) = 0,$$

solution to which is

$$w' \equiv w(t) = w + \frac{\dot{w}(1 - e^{-i\omega t})}{i\omega}.$$

We must reexpress velocities in R in terms of time and initial and final coordinates. In terms of \dot{w} we have

$$\begin{aligned} \dot{w}_0 &= \frac{\omega}{2} \frac{e^{-\frac{i\omega t}{2}} (w - w_0)}{\sin(\frac{\omega t}{2})} \\ \dot{w} &= \frac{\omega}{2} \frac{e^{-\frac{i\omega t}{2}} (w - w_0)}{\sin(\frac{\omega t}{2})} \end{aligned} \quad (\text{S.61})$$

Note that

$$\begin{aligned} x\dot{x} + y\dot{y} &= \text{Re } w^* \dot{w} \\ \text{Re } w^* \dot{w}|_0^t &= \frac{\omega}{2 \sin \frac{\omega t}{2}} \left((|w|^2 + |w_0|^2) \cos \frac{\omega t}{2} - 2 \text{Re } w_0 w^* e^{-\frac{i\omega t}{2}} \right) \\ &= \frac{\omega}{2} \left(\cot \left(\frac{\omega t}{2} \right) [(x - x_0)^2 + (y - y_0)^2] + 2(x_0 y - y_0 x) \right) \\ R &= \frac{m(z - z_0)^2}{2t} + \frac{m\omega}{4} \left(\cot \left(\frac{\omega t}{2} \right) [(x - x_0)^2 + (y - y_0)^2] + 2(x_0 y - y_0 x) \right) \end{aligned} \quad (\text{S.62})$$

Solution 33.1 - Dirac delta function, Gaussian representation. To prove that δ_σ converges to a dirac delta function, it is enough to show that it has the following properties:

- $\int_{-\infty}^{\infty} \delta_\sigma(x) dx = 1$
- $\lim_{\sigma \rightarrow 0} \int_{-a}^a f(x) \delta_\sigma(x) dx = f(0)$

for arbitrary $f(x)$ continuous and positive a .

First property is satisfied by the choice of normalisation constant. Second property is verified by the change of variables $y = x / \sqrt{2\sigma^2}$:

$$\lim_{\sigma \rightarrow 0} \int_{-a}^a f(x) \delta_\sigma(x) dx = \lim_{\sigma \rightarrow 0} \frac{1}{\sqrt{\pi}} \int_{-\frac{a}{\sqrt{2\sigma^2}}}^{\frac{a}{\sqrt{2\sigma^2}}} f(\sqrt{2\sigma^2} y) e^{-y^2} dy = f(0)$$

(R. Paškauskas)

Solution 33.2 - Stationary phase approximation.

Main contribution to this integral come from critical points of $\Phi(x)$. Suppose that p is such a nondegenerate critical point, $p : D\Phi(p) = 0$, and $D^2\Phi(p)$ has full rank. Then there is a local coordinate system y in the neighbourhood of p such that $\Phi(p + y) = \Phi(p) - \sum_{i=1}^{\lambda} y_i^2 + \sum_{i=\lambda+1}^d y_i^2$, where λ is the number of negative eigenvalues of $D^2\Phi(p)$. Indeed, if we set $x - p = Ay$, then $\Phi(x) \approx \Phi(p) + \frac{1}{2} y A^T D^2\Phi(p) Ay$. There exist such A that $\frac{1}{2} A^T D^2\Phi(p) A = \text{diag}[\underbrace{-1, \dots, -1}_{\lambda}, \underbrace{+1, \dots, +1}_{d-\lambda}]$. With this change of variables in mind,

we have

$$I = e^{\frac{i\Phi(p)}{\hbar}} \int_{\mathbb{R}^d} e^{\frac{i}{\hbar} (-\sum_{i=1}^{\lambda} y_i^2 + \sum_{i=\lambda+1}^d y_i^2)} |\det A| dy = e^{\frac{i\Phi(p)}{\hbar}} (\pi\hbar)^{d/2} e^{\frac{i\pi}{4}(-2\lambda+d)} |\det A|$$

Furthermore, $(\det A)^2 \det D^2\Phi(p) = 2^d \exp i\pi\lambda$, therefore

$$|\det A| = \frac{2^{d/2} \exp \frac{i\pi\lambda}{4}}{\sqrt{|\det D^2\Phi(p)|}}.$$

Phase factors $\exp i\pi\lambda/2$ and $\exp -i\pi\lambda/2$ cancel out. Substitute $\exp i\pi d/2 = i^{d/2}$.

The result:

$$I = \frac{(2i\pi\hbar)^{d/2} e^{\frac{i\Phi(p)}{\hbar}}}{\sqrt{|\det D^2\Phi(p)|}}$$

Critical nondegenerate points are isolated. Therefore if Φ has more than one critical point, then equivalent local approximation can be made in the neighbourhoods of each critical point and the complete approximation to the integral made by adding contributions of all critical points.

Answer:

$$I = \sum_{p: D^2\Phi(p) \neq 0} \frac{(2\pi\hbar)^{d/2} e^{\frac{i\Phi(p)}{\hbar}} A(p)}{\sqrt{|\det D^2\Phi(p)|}}$$

Rytis Paškauskas

Solution 33.2 - Stationary phase approximation.

values of x of stationary phase, the points for which the gradient of the phase vanishes

$$\frac{\partial}{\partial x} \Phi(x) = 0.$$

Intuitively, these are the important contributions as for $\hbar \rightarrow 0$ the phase $\Phi(x)/\hbar$ grows large and the function $e^{i\Phi(x)/\hbar}$ oscillates rapidly as a function of x , with the negative and positive parts canceling each other. More precisely, if the stationary points are well separated local extrema of $\Phi(x)$, we can deform the integration contour and approximate $\Phi(x)/\hbar$ up to the second order in x by

$$I \approx \sum_n A(x_n) e^{i\Phi(x_n)/\hbar} \int d^d x e^{\frac{i}{\hbar}(x-x_n)^T D^2\Phi(x_n)(x-x_n)},$$

The second derivative matrix is a real symmetric matrix, so we can transform it to a diagonal matrix by a similarity transformation

$$\text{Diag}(\lambda_1, \dots, \lambda_d) = \mathbf{O} D^2 \Phi \mathbf{O}^+,$$

where \mathbf{O} is a matrix of an orthogonal transformation. In the related coordinate system $u = \mathbf{O}(x - x_n)$ and the integral takes form

$$I \approx \sum_n A(x_n) e^{i\Phi(x_n)/\hbar} \int d^d u e^{i\sum_{k=1}^d \lambda_k u_k^2 / 2\hbar},$$

where we used the fact that the Jacobi determinant of an orthogonal transformation is $\det \mathbf{O} = 1$. Carrying out the Gauss integrals

$$\int du e^{i\lambda u^2 / 2\hbar} = \frac{(2\pi\hbar)^{1/2}}{\sqrt{\lambda}} \tag{S.63}$$

and using $\det D^2\Phi(x_n) = \prod_{k=1}^d \lambda_k$, we obtain the stationary phase estimate of (33.53).

A nice exposition of the subject is given in ref. [32.10].

Solution 33.10 - D-dimensional free particle propagator. A free particle reaches q from q' by only one trajectory. Taking this into account the semiclassical Van Vleck propagator is

$$K_{\text{sc}}(q, q', t) = \frac{e^{i\Phi}}{(2\pi\hbar)^{d/2}} \left| \det \frac{\partial^2 R}{\partial q_i \partial q'_j} \right|^{1/2}$$

The principal function of free motion in D -dimensions is

$$R(q, q', t) = \frac{m}{2I} \sum_{\mu=1}^D (q_\mu - q'_\mu)^2$$

The derivative is

$$\frac{\partial^2 R}{\partial q_i \partial q'_j} = -\delta_{ij} \frac{m}{I}$$

According to that determinant is

$$\left| \det \frac{\partial^2 R}{\partial q_i \partial q'_j} \right|^{1/2} = e^{i\pi D/2} \left(\frac{m}{I} \right)^{D/2},$$

and the Van Vleck propagator is

$$K_{\text{sc}}(q, q', t) = e^{i\pi D/4} \left(\frac{m}{2\pi\hbar I} \right)^{D/2} \prod_{\mu=1}^D \exp \left[\frac{im}{2\hbar I} (q_\mu - q'_\mu)^2 \right]$$

The next step is to calculate the exact quantum propagator:

$$K(q, q', t) = \sum_n \phi_n(q) e^{-iE_n t/\hbar} \phi_n^*(q')$$

Taking that particle wave function in free space is

$$\phi_p(q) = \frac{1}{(2\pi\hbar)^{D/2}} e^{ipq/\hbar}$$

we derive that propagator K is

$$\frac{1}{(2\pi\hbar)^D} \int e^{-\frac{iE}{\hbar} p^2 + ip(q-q')/\hbar} d^D p$$

We can split multi-dimensional integral that stands here into a product of one dimensional integrals. Then we should change variables for purpose of reduction to Poisson-type integrals. We have omitted some straightforward algebra. The result is that the semiclassical Van Vleck propagator and the exact quantum propagator are identical:

$$K(q, q', t) = e^{imD/4} \left(\frac{m}{2\pi\hbar t} \right)^{D/2} \prod_{\mu=1}^D \exp \left[\frac{im}{2\hbar} (q_{\mu} - q'_{\mu})^2 \right] = K_{\text{ex}}(q, q', t)$$

This result could have been anticipated because approximate formula (???.37) becomes exact for the free particle Lagrangian.
 (R. Paškauskas)

Chapter 34. Semiclassical quantization

Solution 34.1 - Monodromy matrix from second variations of the action. If we take two points in the configuration space q and q' connected with a trajectory with energy E and vary them in such a way that the variation of their initial and final points are transverse to the velocity of the orbit in that point, we can write the variations of the initial and final momenta as

$$\delta p_{\perp i} = \frac{\partial^2 S(q, q', E)}{\partial q_{\perp i} \partial q_{\perp k}} \delta q_{\perp k} + \frac{\partial^2 S(q, q', E)}{\partial q_{\perp i} \partial q'_{\perp k}} \delta q'_{\perp k} \quad (\text{S.64})$$

and

$$\delta p'_{\perp i} = - \frac{\partial^2 S(q, q', E)}{\partial q'_{\perp i} \partial q_{\perp k}} \delta q_{\perp k} - \frac{\partial^2 S(q, q', E)}{\partial q'_{\perp i} \partial q'_{\perp k}} \delta q'_{\perp k}. \quad (\text{S.65})$$

Next we express the variations of the final momenta and coordinates in terms of the initial ones. In the obvious shorthand we can write (S.65) as

$$\delta q_{\perp} = -S_{q'q}^{-1} S_{q'q} \delta q'_{\perp} - S_{q'q}^{-1} \delta p'_{\perp},$$

From (S.64) it then follows that

$$\delta p_{\perp} = (S_{qq'} - S_{qq} S_{q'q}^{-1} S_{q'q}) \delta q'_{\perp} - S_{qq} S_{q'q}^{-1} \delta p'_{\perp}. \quad (\text{S.66})$$

These relations remain valid in the $q' \rightarrow q$ limit, with q on the periodic orbit, and can also be expressed in terms of the monodromy matrix of the periodic orbit. The monodromy matrix for a surface of section transverse to the orbit within the constant energy $E = H(q, p)$ shell is

$$\begin{aligned} \delta q_{\perp} &= M_{qq} \delta q'_{\perp} + M_{qp} \delta p'_{\perp}, \\ \delta p_{\perp} &= M_{pq} \delta q'_{\perp} + M_{pp} \delta p'_{\perp}. \end{aligned} \quad (\text{S.67})$$

In terms of the second derivatives of the action the monodromy matrix is

$$\begin{aligned} M_{qq} &= -S_{q'q}^{-1} S_{q'q}, & M_{qp} &= -S_{q'q}^{-1}, \\ M_{pq} &= (S_{qq'} - S_{qq} S_{q'q}^{-1} S_{q'q}), & M_{pp} &= -S_{qq} S_{q'q}^{-1}, \end{aligned}$$

and vice versa

$$\begin{aligned} S_{qq} &= M_{pp} M_{qp}^{-1}, & S_{qq'} &= M_{pq} - M_{pp} M_{qp}^{-1} M_{qq}, \\ S_{q'q} &= -M_{qp}^{-1}, & S_{q'q'} &= -M_{qp}^{-1} M_{qq}. \end{aligned}$$

Now do exercise ??.

Solution ?? - Stationary phase approximation in higher dimensions. In this case $1/h$ is assumed to be a very large number, parameter. The idea of this method is that we only evaluate part of integral I where $e^{i\Phi}$ is stationary i.e., $\varphi \approx \text{const}$. That means we need extrema (saddle points) of manifold Φ . In this case

$$\frac{\partial \Phi}{\partial x_{\nu, \mu}} = 0$$

Introduce a new d -dimensional variable s such, that

$$i\Phi(x) = i\Phi(x_{sp, \mu}) - s^2$$

Integral I in terms of new variables is

$$I = \sum_n e^{i\Phi(x_n)/h} \int e^{-s^2/h} A(x_n(s)) \left| \frac{Dx}{Ds} \right| d^d s$$

Here n sums all stationary phase points which the path of integration (in complex plane) meets. next, we need to calculate the Jacobian J :

$$J = 1 / \left| \frac{\partial s_1}{\partial x_k} \right|,$$

where

$$\frac{\partial s_1}{\partial x_k} = \frac{1}{2i s_1} \frac{\partial \Phi}{\partial x_k}.$$

This expression is undetermined at stationary phase points, because its right hand side becomes division zero by zero. However, by the chain rule

$$\frac{\partial s_1}{\partial x_k} = \frac{1}{2i} \frac{\partial \Phi^2}{\partial s_1} \frac{\partial s_1}{\partial x_k} \frac{\partial s_1}{\partial x_m}$$

where $x = x_{sp}$ are evaluated at the stationary phase point. From this expression we obtain that

$$\left[\frac{\partial s_1^2}{\partial x} \right]_{1,k} = \frac{1}{2i} \frac{\partial \Phi^2}{\partial x_1} \frac{\partial x_k}{\partial x_1}$$

So the Jacobian is (employing a standard notation for a second derivative)

$$J = \frac{(2J)^{d/2}}{\sqrt{\det D^2 \Phi}}.$$

Since the exponential factor $e^{-s^2/h}$ cuts integration sharply because of a very large parameter $1/h$, the function is evaluated only at the stationary point $s = 0$, and the integral is approximately

$$I \approx \sum_n e^{i\Phi(x_n)/h} A(x_n) \frac{(2i)^{d/2}}{\sqrt{\det D^2 \Phi(x_n)}} \int e^{-s^2/h} d^d s$$

Limits of integration may depend on particular situation. If limits are infinite, then

$$\int e^{-s^2/h} d^d s = \left(\int_{-\infty}^{\infty} e^{-s^2/h} ds \right)^d = (\pi h)^{d/2}$$

We substitute this into I and get the answer.

(R. Paškauskas)

Solution ?? - Jacobi gymnastics. We express the Jacobi matrix elements in $\det(\mathbf{1} - \mathbf{J})$ with the derivative matrices of S

$$\det(\mathbf{1} - \mathbf{J}) = \det \begin{pmatrix} I + S_{qq}^{-1} S_{q'q} & S_{q'q}^{-1} \\ -S_{qq'} + S_{qq} S_{q'q}^{-1} S_{q'q} & I + S_{qq} S_{q'q}^{-1} \end{pmatrix}.$$

We can multiply the second column with $S_{q'q}$ from the and subtract from the first column, leaving the determinant unchanged

$$\det(\mathbf{1} - \mathbf{J}) = \det \begin{pmatrix} I & S_{q'q}^{-1} \\ -S_{qq'} - S_{q'q} & I + S_{qq} S_{q'q}^{-1} \end{pmatrix}.$$

Then, we multiply the second column with $S_{q'q}$ from the right and compensate this by dividing the determinant with $\det S_{q'q}$

$$\det(\mathbf{1} - \mathbf{J}) = \det \begin{pmatrix} I & I \\ -S_{qq'} - S_{q'q} & S_{q'q} + S_{qq} \end{pmatrix} / \det S_{q'q}.$$

Finally we subtract the first column from the second one

$$\det(\mathbf{1} - \mathbf{J}) = \det \begin{pmatrix} I & 0 \\ S_{qq'} + S_{q'q} & S_{qq'} + S_{q'q} + S_{qq} \end{pmatrix} / \det S_{q'q}.$$

The last determinant can now be evaluated and yields the desired result (34.2)

$$\det(\mathbf{1} - \mathbf{J}) = \det(S_{qq'} + S_{q'q} + S_{qq}) / \det S_{q'q}.$$

Chapter 35. Quantum scattering

Solution 35.2 - The one-disk scattering wave function.

$$\psi(\vec{r}) = \frac{1}{2} \sum_{m=-\infty}^{\infty} \left(H_m^{(2)}(kr) - \frac{H_m^{(2)}(ka)}{H_m^{(1)}(ka)} H_m^{(1)}(kr) \right) e^{im(\Phi_r - \Phi_k)}. \quad (\text{S.68})$$

(For $r < a$, $\psi(\vec{r}) = 0$ of course.)

(Andreas Wirzba)

Chapter 37. Helium atom

(No solutions available.)

Chapter 38. Diffraction distraction

(No solutions available.)

Chapter B. Linear stability

Solution B.1 - Real representation of complex eigenvalues.

$$\frac{1}{2} \begin{pmatrix} 1 & 1 \\ -i & i \end{pmatrix} \begin{pmatrix} \lambda & 0 \\ 0 & \lambda^* \end{pmatrix} \begin{pmatrix} 1 & i \\ 1 & -i \end{pmatrix} = \begin{pmatrix} \mu & -\omega \\ \omega & \mu \end{pmatrix}.$$

(P. Cvitanović)

Chapter F. Implementing evolution

(No solutions available.)

Chapter D. Symbolic dynamics techniques

(No solutions available.)

Chapter E. Counting itineraries

Solution E.1 - Lefschetz zeta function. Starting with dynamical zeta function ref. [15.13] develops the Atiyah-Bott-Lefschetz fixed point formula and relates it to Weyl characters. Might be worth learning.

Chapter H. Discrete symmetries of dynamics

Solution H.1 - Am I a group? I'm no group because $(ab)c = a \neq a(bc) = c$ breaks the associativity requirement.

W.G. Harter [4.15]

Solution H.2 - Three coupled pendulums with a C_2 symmetry. Consider 3 pendulums in a row: the 2 outer ones of the same mass m and length l , the one midway of same length but different mass M , with the tip coupled to the tips of the outer ones with springs of stiffness k . Assume displacements are small, $x_i/l \ll 1$.

(a) Show that the acceleration matrix $\ddot{\mathbf{x}} = -\mathbf{a}\mathbf{x}$ is ...: Just do it.

(b) Check that $[\mathbf{a}, \mathbf{R}] = 0$, i.e., that the dynamics is invariant under $C_2 = \{e, R\}$, where \mathbf{R} interchanges the outer pendulums: Just do it.

(c) Associated with roots $\{\lambda^{(+)}, \lambda^{(-)}\} = \{1, -1\}$ are the projection operators (B.28)

$$\mathbf{P}_+ = \frac{1}{2} \begin{pmatrix} 1 & 0 & 1 \\ 0 & 20 & 0 \\ 1 & 0 & 1 \end{pmatrix}, \quad \mathbf{P}_- = \frac{1}{2} \begin{pmatrix} 1 & 0 & -1 \\ 0 & 0 & 0 \\ -1 & 0 & 1 \end{pmatrix}.$$

The 3-pendulum system decomposes into a $\text{tr} \mathbf{P}_- = 1$ and $\text{tr} \mathbf{P}_+ = 2$ subspaces. On the 1 - dimensional \mathbf{P}_- yields eigenvalue $(\omega^{(-)})^2 = a + b$. On the 2-dimensional subspace the acceleration matrix is

$$\mathbf{a}^{(+)} = \begin{bmatrix} a+b & -\sqrt{2}a \\ -\sqrt{2}c & c+b \end{bmatrix}.$$

The exercise is simple enough that you can do it without using the symmetry, so: construct $\mathbf{P}^{(+)}$, $\mathbf{P}^{(-)}$ first, use them to reduce \mathbf{a} to irreps, then proceed with computing remaining eigenvalues of \mathbf{a} .

(d) Does anything interesting happen if $M = m$? No, no new symmetry or eigenvalue degeneracy arises from the equal masses case, for any other choice of (non-vanishing, positive) masses.

Solution H.3 - Lorenz system in polar coordinates: dynamics. No solution available.

Solution H.4 - Laplacian is a non-local operator. none available

Solution H.5 - Lattice Laplacian diagonalized. none available

Solution H.6 - Fix Predrag's lecture od Feb 5, 2008. none available

Chapter G. Applications

Solution G.1 - Using the multiplicative property of the Jacobi matrix we can write

$$\Lambda^{t+1}(x_0, \mathbf{u}_0) = \|\mathbf{J}^{t+1}(x_0) \mathbf{u}_0\| = \|\mathbf{J}^t(x(t)) \mathbf{J}^1(x_0) \mathbf{u}_0\|.$$

We can introduce the time evolved unit vector

$$\mathbf{u}(t) = \mathbf{J}^t(x_0) \mathbf{u}_0 / \|\mathbf{J}^t(x_0) \mathbf{u}_0\|.$$

Then

$$\|\mathbf{J}^t(x(t)) \mathbf{J}^1(x_0) \mathbf{u}_0\| = \|\mathbf{J}^t(x(t)) \mathbf{u}(t)\| \|\mathbf{J}^1(x_0) \mathbf{u}_0\|,$$

which is the desired result.

We have to adjoin the tangent space, since the stretching factor depends on \mathbf{u} and not just on x . The stretching factor is multiplicative along the entire trajectory $(x(t), \mathbf{u}(t))$. However, it is not multiplicative along the state space trajectory $x(t)$ with a fixed \mathbf{u} .

Solution G.2 - If $b = a^2$ and $T_b = 2T_a$, we can introduce the variable $y = e^{Jt}$. The dynamo rate equation then reads

$$0 = 1 - x + x^2.$$

The solutions of this are $x_{\pm} = (1 \pm i\sqrt{3})/2$. The dynamo rate is then a complex conjugate pair $\gamma = \log x_{\pm}/T_a$.

The escape rate equation is

$$0 = 1 - x/a - x^2/a^2.$$

The solutions are $x_{\pm} = a(-1 \pm \sqrt{5})/2$. The escape rate is $\gamma = \log(x_{\pm})/T_a$.

In the reverse case the escape rate remains unchanged, while the dynamo rate becomes $\gamma = \log((\sqrt{5} + 1)/2)/T_a$. In this case the advected field grows with an exponential rate. In the previous case it shows oscillations in addition to the exponential growth due to the imaginary part of the rate.

Chapter J. Infinite dimensional operators

Solution J.1 - Norm of exponential of an operator. No solution available.